UTRECHT UNIVERSITY
Graduate school of natural sciences

Master's thesis: Climate Physics

The influence of tides and river discharge on the morphodynamics and the stability of channel systems in deltas using a 0D model

First examiner:
Dr. Maarten van der Vegt

Second examiner:
Prof. Dr. Huib de Swart

Candidate:
Lotje Räkers
1084925

April 20, 2024

Abstract

Approximately 600 million people live or work in a delta and many megacities are located in deltas. Most deltas formed after the last ice age after the sea level stabilised. Many deltas undergo changes due to human actions like dredging and hydropower dams being built. Therefore it is important to have a good understanding of how the morphodynamics and the stability of deltas are determined by the forcings and the initial geometry. A 0D model with a hydrodynamical and a morphodynamical part is used for researching three different channel systems: a one-channel system, a branching channel system and a branching channel system with a connecting channel. A series of simulations for a one-channel system showed that an increasing tidal amplitude and channel length results in an increasing width of the channel mouth. The widest channel mouths are found in channels with a moderate channel depth and river discharge forcing. The branching of a channel leads to lower equilibrium widths. The stability of the found equilibrium widths is researched by perturbing the downstream channels and letting the width or depth evolve afterwards. This showed that tides have a stabilising effect, as found in previous studies. Also, an evolving width did show to have a stabilising effect. More research needs to be done to find out if this is due to the assumptions made or if it is a physical trait. The addition of a connecting channel between the two downstream channels allowed periodic behaviour to form for moderate Shields stresses. However, the underlying reasons behind this periodic behaviour require further research to determine whether they stem from model parameterizations or physical phenomena. At low Shields stresses, the connecting channel has a destabilising effect and at high Shields stresses a stabilising effect.

Acknowledgements

I would like to thank both my supervisors, Maarten van der Vegt and Huib de Swart, for their help throughout the whole process. I really appreciate the weekly meetings that we had where they always took their time discussing the results and helping me with the problems I encountered. I also would like to thank Arya Iwantoro, who helped me find a missing piece in the code. Without him, it would have taken me a lot more time.

Contents

1. Introduction

Deltas are areas of land where rivers meet the ocean. They are shaped by the flow of water and the movement of sediment. Deltas are also affected by tides, waves, storms, and changes in sea level (Hoitink et al., 2016). Most deltas formed after the last ice age around 6000 years ago when the sea level stabilized. Approximately 600 million people live or work in a delta and many megacities like Shanghai, Bangkok and Dhaka are located in deltas (Safra de Campos et al., 2020; Woodroffe et al., 2006). Fisheries and agriculture play an important role. They both provide a big part of the food for the people living close to or in deltas. Deltas are very fertile and practical for agriculture due to the fine-grained river sediments and the flat topography (Rogers et al., 2013). Additionally, deltas are of economic value due to their harbours, which connect inland regions to the rest of the world.

Deltas undergo a lot of changes due to human actions. The Mekong for example has already 160 hydropower dams and many more are being built or are planned to be built (Cowan, 2023; Eslami et al., 2019). Additionally deepening of channels and related maintenance is widely practised. Every year tens of megatons of sand are removed and used for constructing new buildings and roads (Rousseau et al., 2023). Climate change also plays a role altering precipitation patterns, discharge due to glacier melt, and the sea level. These changes affect the tides, river flow, sediment transport, and consequently, the morphology of the delta. Undergoing so many changes and being a vulnerable area for flooding due to its low topography, it is important to have a good understanding of what determines the width and depth of channel networks in deltas.

Depending on the strength of the river discharge, the tides, and the waves deltas have different shapes and sizes (Nienhuis et al., 2018). The main three types are given in Figure 1.1. The first one is a wave-dominated delta, the second one is a river-dominated delta, and the last one is a tide-dominated delta.

(a) **(b)** **(c)**

Figure 1.1: Three types of deltas.

Wave-dominated deltas, such as the Eel Delta, have triangular shapes. The stronger the waves and current along the coast, the smaller the shoreline angle. River-dominated deltas, such as the Wax Lake Delta, typically have a channel network branching outward from a

single main channel, resulting in a fan-like shape. Many of these channels are connected by a connecting channel. These deltas often have a smooth, rounded shoreline. Tide-dominated deltas, like the Mekong Delta, are networks consisting of branching and connecting channels. They tend to have long, finger-like channels and a rounded coast. The influence of tides causes the channels to widen at the river mouth, this is not seen in wave- and river-dominated deltas (Nienhuis et al., 2018).

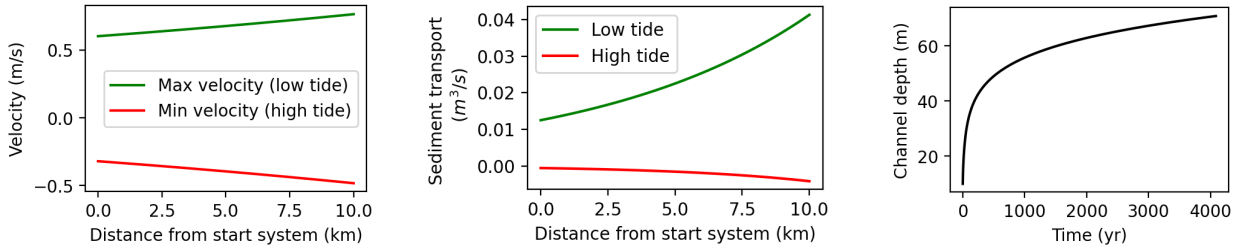

Figure 1.2: (a) Velocity in a channel with a length of 10 km, a depth of 10 m and a constant width of 500 m. The amplitude of the tides is 2 m and the river discharge is 5000 m^3/s. All the used parameters are given in Table 2.4. The riverward boundary is at x=0 km and the seaward boundary is at x=10 km. (b) as (a) but the sediment transport is plotted. (c) as (a) but the change in depth over time is shown.

Taking the Mekong Delta and the Wax Lake Delta as an example, we can highlight some important features, like the widening of the channel mouth and the branching and connecting channels. The widening of the channel mouth is caused by the influence of tides. High tide causes the velocity in a channel to lower, while low tide does the opposite (see Fig. 1.2a). Sediment transport is proportional to the flow velocity to the power five. Because of this, there is more extra sediment transport during low tide compared to the lowering of sediment transport during high tide as seen in Figure 1.2b. If the channel has a constant width, the tides dampen while travelling into the channel because of bottom friction. Therefore the net sediment transport at the seaward boundary would be higher than the net sediment transport at the riverward boundary and erosion would take place causing the channel to deepen (see Fig. 1.2c). The only way to have an equilibrium net sediment transport at both the seaward and riverward boundary is if the channel has a convergent shape. Then the tides dampen less over the length of the channel and the river discharge is spread over a larger area at the seaward boundary lowering the velocity. How much wider the channel mouth gets depends on the strength of the tides. The strength of the tides can be measured as the tidal dominance ratio which is the ratio between the maximum tidal discharge and the river discharge (Nienhuis et al., 2018). Another option for predicting the channel width is using hydraulic geometry and separating the tidal and river discharge (Sassi et al., 2012; Hagen, 2022).

In the Mekong Delta, the Mekong River and Hau River come together at Phnom Penh before splitting up again. Both channels branch into a total of seven channels before flowing into the South China Sea. Having so many branching channels suggests that there is a quasi-

stability that keeps both downstream channels open. In a branching sand river, the network goes back to a stable symmetrical equilibrium after a perturbation at low Shields stresses (Bolla Pittaluga et al., 2015a). For moderate Shields stresses the network goes to a stable asymmetrical equilibrium and for high Shields stresses one of the downstream channels fills up. The Shields stress is a non-dimensional bed shear stress depending on the velocity, the drag coefficient, and the median grain size (Soulsby, 1997) (see Eq. 2.10a). The point where the channel network goes from a symmetrical equilibrium to an asymmetrical equilibrium is called the bifurcation point. The bifurcation does not always take place at the same Shields stress. The width-to-depth ratio and the slope have an influence on the moment when the bifurcation takes place. When the width-to-depth ratio is high, the bifurcation takes place at a low Shields stress compared to when the width-to-depth ratio is low. A steeper channel network bifurcates at lower Shields stresses compared to a channel network with a lower slope (Iwantoro et al., 2021).

Observations in nature show that many of the tide-influenced branching channels are very close to being symmetrical. Examples of that are found in the Mekong Delta (see Fig. 1.3a), the Mahakam Delta (Sassi, 2013) and the Berau River Delta (Buschman et al., 2013). The influence of tides make the stable equilibrium solutions of a channel network less asymmetrical and the network stays longer symmetrical before it bifurcates (Ragno et al., 2020; Iwantoro et al., 2020a; Iwantoro et al., 2020b). The network becomes more symmetrical as the tides grow stronger and the downstream channels shorten. When the tides are strong enough to reverse the flow, the range of symmetrical stable solutions initially increases before decreasing again (Iwantoro et al., 2022).

(a) Example of nearly symmetrical branching channel in the Mekong Delta.

(b) Example of connecting channel in the Wax Lake Delta.

Figure 1.3

When a river splits up into two, the two downstream channels can be connected through a connecting channel. This happens in the Wax Lake Delta (see Fig. 1.3b) and many more as the Mekong Delta, the Yangtze Delta, the Dongjiang Delta and the Hanjiang Delta (Gao et al., 2023). Adding a connecting channel influences the hydrology of the channel network. The connecting channel adds an extra order of freedom to the water levels of the downstream channels (Gao et al., 2023). With the connecting channel, the discharge asymmetry right after the junction decreases while the discharge asymmetry downstream of the connecting

channel increases.

The main goal is to understand how tides and river discharge determine the widths and depths of deltaic channel systems. Because of the wide range of possible network configurations and forcing conditions, I aim to develop a simple morphodynamic, physics-based model that is able to capture the essential dynamics but is computationally efficient. I decided to develop a 0D model in which both width and depth can evolve. The studies mentioned before all used prescribed width profiles and mainly studied depth evolution using 1D and 2D models solving those analytical or numerical, but most channels show a wider variability in width than in depth. Because no one has used a 0D model with a width that can evolve to study channel networks, I first looked at the stability of one channel under the influence of tides letting the width evolve. After that, I researched a more complex system having a branching channel. There I looked at whether it would make a difference if, after a perturbation, the width or depth was allowed to evolve. Lastly, I added a connecting channel between the two downstream channels adding to its complexity. The hydrodynamics of a network like this has been studied before but not its morphodynamics. The influence of tides was removed to keep it easier to understand all the processes going on. Adding tides to this network would be the next step but I could not do this due to time constraints. This resulted in three research questions that will be answered in this report.

1. How does the widening of a channel under the influence of tides depend on the strength of the tides, the river discharge, the channel depth and the channel length?
2. How do tides influence the stability of a branching channel with an evolving width or depth?
3. What is the difference in stability between a branching channel with and without a connecting channel?

The second chapter will discuss the model. Following this, each research question will have its own section explaining the research methodology. Chapter three will present the results for each research question, which will then be discussed in chapter four. The final chapter will provide a summary of the most important findings.

2. Method

2.1 Model

The goal is to make a time efficient and simple model to research the equilibrium morphology and the stability of different channel networks. The channel networks that are being researched are shown in Figure 2.1. The number of the channel system correspondences with the number of the research question. Each channel has a width, b, depth, h, and length, L. The length is kept constant in space and time, the depth is constant in space but not in time and the width is allowed to vary both in space and time. The width profile is prescribed by $b = b_L exp(\gamma(x - L))$, where b_L is the channel width at the seaward end of the channel at x=L, $\gamma = -ln\left(\frac{b_0}{b_L}\right)/L$ is the inverse e-folding length and b_0 is the channel width at the riverward end of the channel at x=0. Water flows trough the channels. The water flow is calculated by solving the cross-sectionally averaged shallow water equations (SWE) following Alebregtse et al. (2016). The sediment transport is calculated by the Engelund and Hansen sediment transport equation (Hansen et al., 1972) using the velocity at the start and end of each channel. At the junctions, the sediment transport of the upstream channel is divided between the two downstream channels using the Nodal Point relation of Bolla Pittaluga et al. (2003). With the sediment transport at the start and end of each channel, the change in morphology can be calculated. The change in morphology influences the hydrodynamics, creating a loop that continues until the network reaches an equilibrium solution where the morphology of the network does not change anymore.

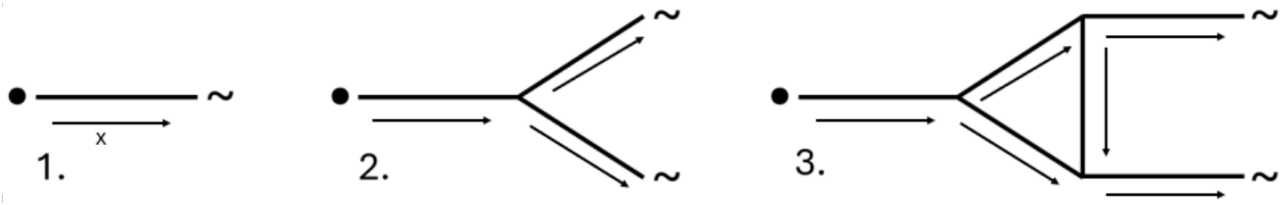

Figure 2.1: Overview of 3 channel systems that are being researched. The dots show the boundaries connected to land and the tildes show the boundaries connected to the sea. The arrows show the direction of the x-axis.

2.1.1 Hydrodynamics

In an estuary, the tidal and river flow interact with each other. To simplify the solutions a number of assumptions are made. The average flow induced by river discharge is assumed to dominate over various nonlinear interactions that may contribute to residual currents. Consequently, we neglect many nonlinear interactions and focus on dominant mechanisms.

While there exists non-linear river-tide interaction, it primarily occurs through the frictional term. Taking the assumptions into account, the SWE can be simplified to

$$\frac{\partial u}{\partial t} = -g\frac{\partial \eta}{\partial x} - \frac{\lambda u}{h}, \tag{2.1a}$$

$$b\frac{\partial \eta}{\partial t} + h\frac{\partial}{\partial x}(bu) = 0, \tag{2.1b}$$

where u is the along-channel cross-sectionally averaged velocity, t is the time, x is the along-channel distance counting from the riverward end of the channel, g is the gravitational acceleration, η is the free surface elevation and λ is the effective friction coefficient. An overview of all used variables and parameters is given in appendix A.

Each channel end can be connected to land, to the ocean or to other channels. Boundary conditions are prescribed for all three possibilities. The boundary conditions of the landward boundary are given in Equation 2.2a, the seaward boundary in Equation 2.2b and the junctions in Equation 2.2c.

$$x = 0, j = 0 : bhu = Qr, \tag{2.2a}$$

$$x = L, j \in O : \eta_j = N\cos(\sigma t - \phi), \tag{2.2b}$$

$$\forall j,k \in J \quad \begin{cases} g\eta_j + \frac{1}{2}u_j^2 & = g\eta_k + \frac{1}{2}u_k^2, \\ \sum_{j\in J} b_j h_j \mathcal{U}_j & = 0, \end{cases} \tag{2.2c}$$

where j is the channel index, Qr is the prescribed river discharge, O are all the channels connected to the ocean, N and ϕ are the amplitude and phase of the tidal wave, σ is the tidal frequency and J are all the channels connected in the junction under consideration.

For finding the solutions of equations 2.1 Alebregtse et al. (2016) with some small deviations is followed. In Alebregtse et al. (2016), the set of equations is solved semi-analytical by

performing a harmonic truncation.

The water flow is split into two harmonic components, the residual component, M0, and the semi-diurnal one, M2. A random variable describing the flow can be split into the harmonic components in the following way $\chi = \chi_{M0} + \chi_{M2}$. The subscripts refer to the M0 and M2 components respectively. From now on in this section, the subscripts refer to the harmonic component first and then the channel index. For example $\chi_{M2,4}$ is the semi-diurnal component in channel four of variable χ.

The leading order solutions of the SWE for the different components are the ordinary differential equations below.

$$u_n = \frac{-gh}{\lambda_n - ia\sigma h}\frac{\partial \eta_n}{\partial x}, \tag{2.3a}$$

$$-ia\sigma\eta_n = -\frac{1}{b}\frac{\partial}{\partial x}bu_n, \tag{2.3b}$$

where $a = 0, 1$ for M0 and M2 respectively and $n = M0, M2$. The Boundary conditions prescribed for the landward boundary (Eq. 2.4a), the oceanward boundary (Eq. 2.4b) and the junctions (Eq. 2.4c) become:

$$x = 0, j = 0 \quad \begin{cases} bhu_{M0} & = Qr, \\ \mathcal{U}_{M2} & = 0, \end{cases} \tag{2.4a}$$

$$x = L, j \in O, \quad \begin{cases} \eta_{M0,j} & = 0, \\ \mathcal{N}_{M2,j} & = N_{M2}\exp(i\phi_{M2}), \end{cases} \tag{2.4b}$$

$$\forall j, k \in J, n = M0, M2 \quad \begin{cases} \mathcal{N}_{n,j} & = \mathcal{N}_{n,k}, \\ \sum_{j\in J} b_j h_j \mathcal{U}_{n,j} & = 0, \end{cases} \tag{2.4c}$$

where $\mathcal{U}$ is the complex velocity of the tidal wave and $\mathcal{N}$ is the complex amplitude of the tidal wave. The last two boundary conditions in Equation 2.2a are only true when the tidal

wave gets reflected at the riverward boundary of the channel network. If the tidal wave does not get reflected, then those two boundary conditions can be ignored because the wave travels only in one direction causing $B = 0$ in Equation 2.5a for the channel connected to the landward boundary.

Solving Equations 2.3 with the boundary conditions in Equations 2.4 results in the following general solutions

$$\mathcal{N}_n = \exp(\gamma x/2)\left(A_n \exp(i\kappa_n x) + B_n \exp(-i\kappa_n x)\right), \tag{2.5a}$$

$$\mathcal{U}_n = \frac{-gh}{\lambda_n - in\sigma h}\frac{d\mathcal{N}_n}{dx}, \tag{2.5b}$$

where A and B are constants that are determined by the boundary conditions and κ is the complex wave number. For the residual component Equation 2.5a can be simplified to $\mathcal{N}_{M0} = A_{M0} + B_{M0}\exp(\gamma x)$.

To transform the found complex amplitude and velocity to the real amplitude and velocity, $u = \Re(\mathcal{U} exp(-i\sigma t))$ and $\eta = \Re(\mathcal{N} exp(-i\sigma t))$ are used where $\Re$ denotes taking the real part of the complex values. The tidal frequency of the quarter-diurnal tides is twice the tidal frequency of the semi-diurnal tides.

In Alebregtse et al. (2016) the space-dependent effective friction coefficient for the residual flow is defined as

$$\bar{\lambda}_{M0} = \frac{16}{15\pi}C_d U\left(1 + 2\left(\left(\frac{|u_{M0}|}{U}\right)^2 + \frac{3}{2}\left(\frac{|\mathcal{U}_{M2}|}{U}\right)^2\right)\right), \tag{2.6a}$$

$$\lambda_{M0} = \frac{1}{L}\int_0^L \bar{\lambda}_{M0} dx, \tag{2.6b}$$

where C_d is the drag coefficient and $U = u_{M0} + |\mathcal{U}_{M2}| + |\mathcal{U}_{M4}|$, the maximum total velocity. The velocity of the residual flow is defined as follows

$$u_{M0} = -\frac{gh}{\lambda_{M0}}\frac{d\eta_{M0}}{dx}. \tag{2.7}$$

The velocity of the residual flow, u_{M0}, depends on the effective friction coefficient, λ_{M0}, and

the other way around. While running the model, this caused a loop wherein they both cancel each other out every other round. To solve this problem the effective friction coefficient used for calculating the residual flow in the model is redefined as

$$\tilde{\lambda}_{M0} = \frac{16}{15\pi} C_d \frac{U}{u_{M0}} \left(1 + 2 \left(\left(\frac{|u_{M0}|}{U} \right)^2 + \frac{3}{2} \left(\frac{|\mathcal{U}_{M2}|}{U} \right)^2 \right) \right), \tag{2.8a}$$

$$\hat{\lambda}_{M0} = \frac{1}{L} \int_0^L \tilde{\lambda}_{M0} dx, \tag{2.8b}$$

and the velocity of the residual flow is redefined as

$$u_{M0} = sign \left(-\frac{gh}{\hat{\lambda}_{M0}} \frac{d\eta_{M0}}{dx} \right) \sqrt{| -\frac{gh}{\hat{\lambda}_{M0}} \frac{d\eta_{M0}}{dx} |}. \tag{2.9}$$

2.1.2 Sediment transport

The sediment transport depends on factors like the velocity, the diameter of the sediment and the drag coefficient (Soulsby, 1997). The sediment transport equation of Engelund and Hansen (see Eq. 2.10) is chosen because it is an easy method that does not take a lot of computational power and it is widely accepted. The sediment transport equation of Engelund and Hansen does not differentiate between bed load en suspended load. The suspended load floats in the water and the bed load rolls, slides, and hops along the channel bed.

$$\theta = C_d \frac{u^2}{(s-1)gd50}, \tag{2.10a}$$

$$Qs = b \frac{0.05}{C_d} \theta^{2.5} \sqrt{(s-1)gd50^3}, \tag{2.10b}$$

where θ is the Shields stress, $s = \rho_s / \rho_w$ is the relative density of the sediment defined as the density of the sediment divided by the density of water, $d50$ is the median diameter of the sediment and Qs is the sediment transport.

At a bifurcation, the sediment from the upstream channel needs to be divided over the two downstream channels. Bolla Pittaluga et al. (2003) derived a physically based nodal

point relation to determine the division in sediment transport.

$$Qs_b = \frac{b_b}{b_b + b_c} Qs_a + Qsy, \tag{2.11a}$$

$$Qs_c = Qs_a - Qs_b. \tag{2.11b}$$

The subscript a strands for the upstream channel and the subscripts b and c are the two downstream channels. Channel b gets a certain amount of sediment transport depending on the discharge distribution and the transverse sediment transport, Qsy (see Fig. 2.2). The transverse sediment flow takes place over a distance αb_a before the branching point and is induced by the bed level differences between the two downstream channels.

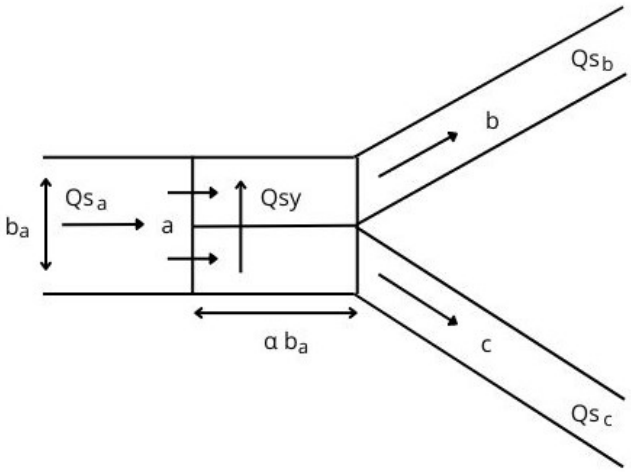

Figure 2.2: Schematic overview of branching channel network and transverse sediment transport.

$$Qsy = Qs_a \left(\frac{Qyh_a}{Q_a \alpha h_{abc}} - \frac{r}{\sqrt{\theta}} \frac{h_c - h_b}{0.5 b_a} \right), \tag{2.12}$$

where $Qy = \frac{1}{2} \left(Q_b - Q_c - Q_a \frac{b_b - b_c}{b_b + b_c} \right)$ is the transverse water discharge and r is a calibration parameter. The average depth, h_{abc}, is calculated by

$$h_{abc} = \frac{b_a h_a + b_b h_b + b_c h_c}{b_a + b_b + b_c}, \tag{2.13}$$

which is the same as in Iwantoro et al. (2021). To make sure that it is not possible to have sediment transport that is in the opposite direction of the water flow, $\frac{Qs}{Q} > 0$. When $\frac{Qs}{Q} < 0$ in one of the two downstream channels, the sediment transport in that channel is set equal to zero and the other downstream channel gets all the sediment from the upstream channel. At a confluence, the sediment transport of the downstream channel is calculated by simply adding the sediment flux of the two upstream channels together so that there is no loss in sediment.

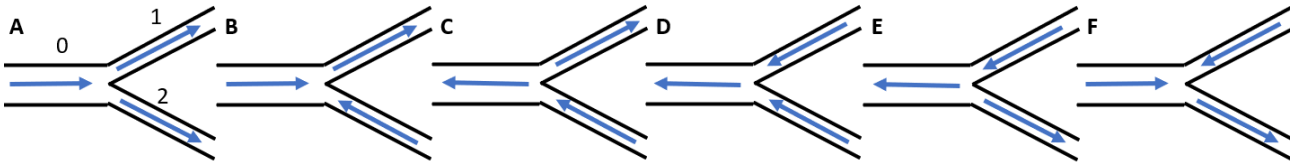

Figure 2.3: The six states a system of three connected channels can have depending on the direction of the flow. The direction of the water flow is given by the blue arrows.

In Figure 2.3 the six different states that a system of three connected channels can have are shown. The states depend on the direction of the water flow. A switch of direction can be caused by tides or one of the channels being a connecting channel. The model looks every time step at the direction of the flow in all channels and then decides in which state the network is and what the correct way of dividing or adding the sediment flux is.

2.1.3 Morphodynamics

When erosion or sedimentation takes place the volume of the channel changes. The change in volume can be calculated by solving

$$(1-p)\frac{dV}{dt} = < Qs_{out} - Qs_{in} >, \tag{2.14}$$

where p is the porosity and $V = h(t)\int_0^L b(x,t)dx$ is the volume of the channel. Taking the mean over a tidal cycle is shown by $<>$. The subscripts out and in stand for the outgoing or incoming sediment transport. Both the width and the depth are able to change in time. When the width and length are assumed constant in time, the change in depth is given by

$$\frac{dh}{dt} = \frac{< Qs_{out} - Qs_{in} >}{(1-p)\int_0^L b(x,t)dx} = \frac{< Qs_{out} - Qs_{in} >}{(1-p)\frac{b_L}{\gamma}\left(1-\exp\left(\gamma(x-L)\right)\right)}. \tag{2.15}$$

Here a cohesionless bed is assumed. Because of this, there is no maximum depth of the channel and the channel can become infinitely deep or shallow if the model does not go to an equilibrium solution. When the depth and length are assumed constant in time, the

change in width can be calculated by solving

$$\frac{d}{dt}\left(\frac{b_L}{\gamma}\left(1-\exp\left(\gamma(x-L)\right)\right)\right)=\frac{<Qs_{out}-Qs_{in}>}{(1-p)h}. \tag{2.16}$$

The morphodynamics is only dependent on the sediment transport that enters and leaves the channel. The model therefore does resemble a box model. The main difference is that the tidal flow depends on the width profile.

2.2 One-channel system

To answer research question 1 four different sets of simulations were performed. The first two sets were chosen to test the sensitivity to the geometry of and forcings working on the channel. In the first set, the channel length and channel depth were varied whereafter the width was allowed to evolve. In the second set, the discharge and tidal amplitude were varied whereafter the width was allowed to evolve. In the third set, a width profile was prescribed and the depth was allowed to evolve. In the last set, the geometry, discharge and tidal amplitude of 36 single-channel estuaries found in nature are used to research how well the model is in capturing the widening of the channels.

2.2.1 Sensitivity analysis

Chosen is to first look at only single-channel estuaries to make it easier to understand the processes going on. For the same reason, the tidal forcing consists of only semi-diurnal tides, so no external forced quarter-diurnal tides. In the model, the tidal wave does not get reflected at the riverward boundary because tidal waves can travel further into channels than the channel lengths that are tested, between 10 and 70 km.

In the first two sets of simulations, the model was set up with a starting geometry and forcings in the form of river discharge and tides (see Tab. 2.1). The depth and length of the channel were kept constant while the width was allowed to evolve following Equation 2.16 until an equilibrium was reached. An equilibrium is reached when $\frac{dV}{dt}=0$. Now that only the width is allowed to change in time an equilibrium is found when $\frac{db}{dt}=0$. The parameters that are not tested are given in Table 2.2.

In the third set of simulations, the width profile was prescribed having an e-folding length scale between 5 and 50. Then the depth was allowed to evolve resulting in an equilibrium depth or the channel closing. This was first done for a channel with the set-up shown in Table 2.1 and parameters in Table 2.2. After that, the moment were the channel does not close off completely anymore is followed for a discharge ranging between 500 and 5000 m^3/s while the tidal amplitude, the starting dimensions of the channel and the parameters are kept the same.

	Qr (m^3/s)	N (m)	L (km)	h (m)	b_0 (m)	b_L (m)
set 1	500-5000	0.2-2	20	10	300	300
set 2	5000	2	10-50	5-30	300	300
set 3	2000	2	20	10	300	depending on e-folding length
set 4	data	data	data	data	data	data

Table 2.1: Forcings and starting geometry used for answering research question 1. The data used for set 4 can be found in appendix C.

Parameter	Value	Unit
C_d	$1/13^2 \approx 0.0059$	
s	2.65	
$d50$	$0.275 * 10^{-3}$	m
g	9.81	m/s^2
p	0.4	
C	$13\sqrt{g}$	$m^{\frac{1}{2}}/s$

Table 2.2: Parameters used answering research question 1.

2.2.2 Application to channels in nature

In the last set of simulations the width is modelled for estuaries observed in nature. The data used are taken from Nienhuis et al. (2018). The total data set had 73 estuaries. Only the single-channel estuaries were used coming to a total of 36. In the data set, the river discharge, the channel depth, the channel length, the tidal amplitude and the channel width at both the riverward boundary and the seaward boundary were given. The river discharge and tidal amplitude were acquired from Syvitski et al. (2007), Cohen et al. (2013) and Egbert et al. (2002). The channel depth is estimated by using hydraulic geometry relations for rivers (Mikhailov, 1970). An overview of all used data is given in appendix C. Some information, like the drag coefficient, was not given in the data set. To keep comparison further on easier, the same settings as in Bolla Pittaluga et al. (2015a) are used (see Tab. 2.4).

The observed and modelled widths were plotted against each other to compare. To qualify the performance of the model, the root mean square deviation (RMSD) was calculated by

$$RMSD = \sqrt{\frac{1}{n}\sum_{i=1}^{n}(b_{Lobs,i} - b_{Lmod,i})^2} / \frac{1}{n}\sum_{i=1}^{n}(b_{Lmod,i}) - 1, \tag{2.17}$$

where the subscript *obs* stand for the observed width and *mod* for the modelled width. The coefficient of determination, r^2, was calculated using a Scipy optimize function in Python. $u_2/u_0 = \frac{|\mathcal{U}_{M2}|}{u_{M0}}$ at the seaward boundary is calculated to learn more about which of the deltas were modelled well and which were modelled poorly. This was calculated at the start of

each simulation, thus for observed widths and not the modelled widths

2.3 Branching channel system

To answer research question 2, the same sensitivity analysis as for research question 1 was done but now for a branching channel. After that, the stability of the found widths was researched by perturbing the system. Lastly, the morphodynamics and stability of one branching channel in the Mekong Delta were researched to determine how well the model performs.

2.3.1 Sensitivity analysis

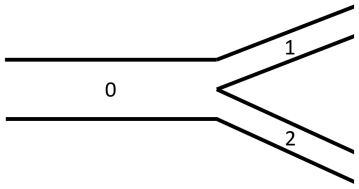

Figure 2.4: Schematic overview of the channel system. The river flows from left to right.

The influence of the discharge, tides, channel depth and length is researched for a one-channel system in section 2.2.1. The same is repeated to see if the results would be different having a branching channel (Fig. 2.4). For finding the equilibrium width the same process is repeated as in section 2.2.1. The forcings and starting dimensions of the channels used are given in Table 2.3 and the used parameters are given in Table 2.4. These parameters are chosen because they are the same as in Bolla Pittaluga et al. (2015a) and Iwantoro et al. (2021).

	Qr (m^3/s)	N (m)	L (km)	h (m)	b_0 (m)	b_1 (m)	b_2 (m)
set 1	5000	2	10-50	5-30	300	150	150
set 2	500-5000	0.2-2	20	10	300	150	150

Table 2.3: Forcings and geometry used for answering research question 2.

The upstream width of channels 1 and 2 can be kept constant or be allowed to evolve so that $b_{0,L} = b_{1,0} + b_{2,0}$, where $b_{0,L}$ is the width of channel 0 at $x = L$ and $b_{1,0}$ and $b_{2,0}$ are the widths of channels 1 and 2 at $x = 0$. Both methods are being researched to investigate if the results would differ. There are different ways of deciding how much each of the upstream widths of channels 1 and 2 are allowed to change, like determining it based on the net sediment transport or using hydraulic geometry relations. I have chosen to calculate the ratio between the net sedimentation/erosion between the two downstream channels because if the erosion in one of the channels is bigger than the other, you want the upstream width of

Parameter	Value	Unit
α	1.5	
r	0.5	
s	2.65	
C_d	$1/13^2 \approx 0.0059$	
$d50$	$0.275 * 10^{-3}$	m
g	9.81	m/s^2
p	0.4	
C	$13\sqrt{g}$	$m^{\frac{1}{2}}/s$

Table 2.4: Parameters used answering research question 2 and 3.

this channel to grow faster than the upstream width of the other channel. This resulted in the set of equations below.

$$\frac{db_{0,0}}{dt} = 0, \tag{2.18a}$$

$$b_{0,L} = b_{1,0} + b_{2,0}, \tag{2.18b}$$

$$\frac{db_{1,0}}{dt} / \frac{db_{2,0}}{dt} = \frac{< Qs_{1,out} - Qs_{1,in} >}{< Qs_{2,out} - Qs_{2,in} >}, \tag{2.18c}$$

$$\forall j \in J \quad \begin{cases} \frac{d}{dt}\left(\frac{b_{j,L}}{\gamma_j}\left(1 - \exp\left(\gamma_j(x - L_j)\right)\right)\right) = \frac{<Qs_{j,out} - Qs_{j,in}>}{(1-p)h_j}, \\ \gamma_j = \ln \frac{b_{j,0}}{b_{j,L}} / L_j. \end{cases} \tag{2.18d}$$

Equation 2.18a makes sure that the upstream width of channel 0 stays constant in time. The sum of the width of channels 1 and 2 should be equal to the width of channel 0 at the junction as in equation 2.18b. How the widths of channels 1 and 2 change depends on the amount of sedimentation or erosion as prescribed in equation 2.18c. For all channels, the new width and inverse e-folding length are calculated by equation 2.18d. In total, this yields nine equations to solve for nine unknowns: b_0, b_L, and γ for each of the three channels.

2.3.2 Stability of found equilibrium widths

Having found the equilibrium widths, their stability can be researched by perturbing the width or depth. The system is stable when $\lim_{t\to\infty}(V + V') = V$, where V' is a perturbation in volume. In other words, the system goes back to its old dimensions overtime after being perturbed. The perturbation can be a small change in depth or width. After the perturbation, the systems width or depth can evolve. This gives a total of eight ways to test the stability of the channel network. All eight ways are tested to see if the results would be different. This is done for a Shields stress range between 0.05 and 3 and a semi-diurnal tidal amplitude of 0 m, 0.5 m, 1 m and 2 m.

	Channel 0	Channel 1	Channel 2
Channel length	10 km	10 km	10 km
Channel depth	10 m	10 m	10 m
Channel width	300 m	150 m	150 m

Table 2.5: Dimensions channel system used to test influence tides.

The morphology of chosen the system is given in Table 2.5. The parameters used are given in Table 2.4.

The discharge asymmetry between the two downstream channels was calculated by

$$\Psi_{Q12} = \frac{Q_1 - Q_2}{Q_0}, \tag{2.19}$$

where Q is the tidally averaged discharge and the subscripts refer to the channel indexes.

2.3.3 Application to a branching channel in the Mekong Delta

In sections 2.3.1 and 2.3.2 more general channel systems and configurations were used to answer research question 2. In this section, the stability of a branching channel was again looked at but then for a part of the Mekong Delta (see Figure 2.5). The starting situation was the channel network with its current morphology taking the mean of both downstream channel widths and lengths so that the system is symmetrical. First, the width was allowed to evolve to an equilibrium width. Whereafter the depth was perturbed and allowed to evolve.

	Channel 0	Channel 1	Channel 2
Channel length	33 km	33 km	33 km
Channel depth	11.2 m	11.2 m	11.2 m
Channel width at x=0	2900 m	1450 m	1450 m

Table 2.6: Dimensions of part of Mekong Delta.

Figure 2.5: Overview of the part of the Mekong Delta that is researched.

At the river mouth, the tides have an amplitude of 1.3 m. The discharge varies between 1200 during the dry season and 16000 m^3/s during the wet season. The annual mean discharge is 8600 m^3/s. The stability was researched for the whole range of discharges and tidal amplitudes of 0, 0.1, 0.3, 0.5 and 1.3 m. The channel lengths and widths are measured using Google Earth. The channel depth, discharge data and tidal amplitude are from Nienhuis et al. (2018) and Eslami et al. (2019). All the other parameters are given in table 2.4. The tides were not reflected at the start of channel 0, because they are able to travel further into the channel network.

2.4 Branching channel network with connecting channel without tides

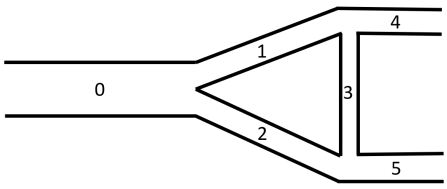

Figure 2.6: Schematic overview of the channel network with connecting channel. The river flows from left to right.

To answer research question 3, we will now look at a system like in Figure 2.6. Adding the connecting channel allows water and sediments to reach the same point via different pathways. This adds to the complexity of the system.

2.4.1 Stability of branching channel network with connecting channel

The influence of a connecting channel on the stability of a branching channel system has never been researched before, therefore the influence of tides is removed to simplify the system. Given the absence of tides, altering the width does not make sense since rivers in equilibrium maintain a consistent width over the whole channel length. Therefore the depth was both perturbed and allowed to evolve. The four ways to perturb the downstream channels are given in Table 2.7. All options give the same final result. Table 2.8 gives an overview of the lengths and widths of each channel. The channel length does not influence the equilibrium but only the timescale as long as the length of all channels are equal. For that reason an arbitrary length can be chosen.

Option #	Depth channel 0	Depth channel 1	Depth channel 2	Depth channel 3	Depth channel 4	Depth channel 5
1	10	10.1	9.9	10	10	10
2	10	10.1	9.9	10	10.1	9.9
3	10	10.1	9.9	10	9.9	10.1
4	10	10	10	10	10.1	9.9

Table 2.7: Ways to perturb a branching river with a connecting channel. All values are given in meters.

	Channel 0	Channel 1	Channel 2	Channel 3	Channel 4	Channel 5
Length (km)	1	1	1	1	1	1
Width (m)	300	150	150	100	150	150

Table 2.8: Dimensions channel network with connecting channel.

The stability was checked for Shields stresses between 0.05 and 3 by changing the river discharge from 580 to 4500 m^3/s. The discharge asymmetry between channels 1 and 2, Ψ_{Q12}, and between channels 4 and 5, Ψ_{Q45}, were calculated as in Equation 2.19. The values of the parameters used were kept the same (see Tab. 2.4).

2.4.2 Impact width of the connecting channel on stability

Also the width of the connecting channel influences the stable solutions of the channel network. The width of the connecting channel was varied between 10 and 100 m to test how big its influence is. The stable solutions were calculated in the same way as in section 2.4.1 but changing the width of the connecting channel to 10, 50 and 100 m. After that, Ψ_{Q12} and Ψ_{Q45} were calculated again.

2.4.3 Application to the Wax Lake Delta

The Wax Lake Delta is one of the deltas with a connecting channel. The connecting channel in the Wax Lake Delta influences the discharge distribution between the Campground pass,

Figure 2.7: Overview of the Wax Lake Delta.

channels 2 and 5, and the other channels in the delta (see Fig. 2.7). How big this influence is was tested by modelling the Wax Lake Delta with and without the connecting channel.

	Channel 0	Channel 1	Channel 2	Channel 3	Channel 4	Channel 5
Length (km)	1.8	1.9	2.1	1.1	7.6	4.1
Depth (m)	10	8	3	0.5	4	3
Width (m)	300	600	240	70	1800	370

Table 2.9: Dimensions of the Wax Lake Delta. Data from Meselhe et al. (2021) and Google earth.

The channel depths and river discharge are from Meselhe et al. (2021). The discharge is around 1270 m^3/s during the dry season and 3640 m^3/s during the wet season. The annual average is 2520 m^3/s. The tidal amplitude is approx 0.34 m making the tides not strong enough to reverse the flow (Rosen et al., 2013; Shaw et al., 2013). The width and length of the connecting channel are measured using Google Earth.

To see if the network is in equilibrium, the depths were allowed to evolve. This is done for both the case with and without connecting channel.

3. Results

3.1 One-channel system

3.1.1 Default case

The net sediment transport of a channel depends on the strength of the forcings and the dimensions of the channel. To analyse the influence of the tidal amplitude, river discharge, channel length and channel width on a channel's sediment transport, a series of simulations is performed researching a range of each parameter.

The net sediment transport, Qs, can be calculated using Equation 2.10. The net sediment transport and the velocity are related by: $Qs \propto bu^5$ where $u = u_{M0} + u_{M2}$. The net sediment transport consists of three components when splitting up the residual flow velocity, u_{M0}, and the semi-diurnal flow velocity, u_{M2}: $\beta b u_{M0}^5$, $10\beta b u_{M0}^3 u_{M2}^2$ and $5\beta b u_{M0} u_{M2}^4$ where $\beta = \frac{0.05}{Cd}\frac{\Theta^{2.5}}{u}\sqrt{(s-1)gd50^3}$ is a constant independent of space and time. Only three components remain because we look at the tidally averaged sediment transport causing all components with u_{M2}^{2n} and $n \in \mathbb{R}$ to be zero.

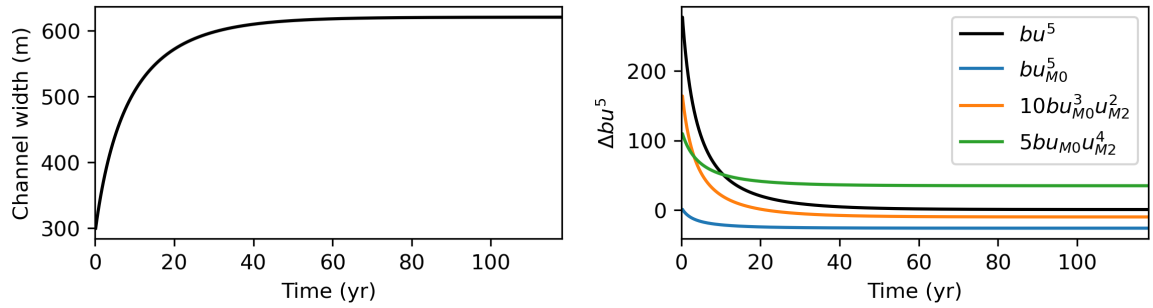

Figure 3.1: (a) Plot of the width of the channel at x=L, b_L. (b) The black line shows the difference of bu^5 at $x = L$ and $x = 0$ over time. For the three components, the same is done. The difference in bu_{M0}^5, $10bu_{M0}^3u_{M2}^2$ and $5bu_{M0}u_{M2}^4$ at the x=0 and x=L are shown by the blue, orange and green lines respectively. In both panels initially $b_L = b_0 = 300$ m, $h = 10$ m and $L = 20$ km. The upstream width, b_0, is kept fixed during the simulation. The discharge, Qr = 2000 m^3/s and the tidal amplitude, N = 2 m. Other parameters are given in Table 2.4.

As is shown in Figure 3.1a, the width at the seaward end of the channel increases in time and becomes approximately constant after 60 years. Thus the system evolves towards a stable morphodynamics equilibrium, in which the sediment transport at $x = L$ equals that at $x = 0$ (see black line in Fig. 3.1b). The explanation of this behaviour is as follows. At the start of the simulation $b_0 = b_L = 300$. When the channel width is constant the residual flow

velocity is constant in the whole channel and therefore the difference in sediment transport due to the residual flow at $x = L$ and $x = 0$ is zero (see blue line in Fig. 3.1b). The semi-diurnal velocity at $x = 0$ is smaller than at $x = L$ due to bottom friction resulting in a higher seaward net sediment transport at $x = L$ than at $x = 0$ (see black line in Fig. 3.1b). This leads to erosion and thus widening of the channel. The increase in width at $x = L$ lowers the residual velocity at $x = L$ resulting in a lowering of sediment transport (see blue line in Fig. 3.1b). The converging shape of the channel increases the semi-diurnal velocity at the landward boundary, at $x = 0$, increasing the sediment transport at the landward boundary making the difference in net sediment transport between the two boundaries smaller. This results in an equilibrium where $b(u_{M0}^5 + 10u_{M0}^3 u_{M2}^2 + 5u_{M0}u_{M2}^4)$ is equal at both boundaries.

3.1.2 Sensitivity analysis

The procedure in section 3.1.1 is repeated for a tidal amplitude ranging between 0.2 and 2 m and a river discharge ranging between 500 and 5000 m^3/s to test the sensitivity of the system.

The higher the amplitude of the semi-diurnal tides the wider the river mouth becomes (see Fig. 3.2a), but the modelled dependence on discharge is more complex. For relatively small tides, up to 0.9 m, increasing discharge results in smaller widths for the channel mouth. For $N > 0.9$ m, there is an increase in width of the channel mouth for increasing discharges up to 950 m^3/s and for larger values a decreasing dependence. This is due to the net sediment transport caused by the residual flow (see Fig. 3.2c). At low discharges, the residual velocity at the landward boundary is relatively low compared to the semi-diurnal velocity. Therefore the net sediment transport caused by residual flow is only a small component of the total net sediment transport at the landward boundary and the net sediment transport due to the semi-diurnal flow does not have to compensate much for the difference in net sediment transport due to the residual flow at $x = 0$ and $x = L$. The channel has to become less convergent. The e-folding length shows the same patterns as b_L/b_0. This is because the channel length is kept constant in all simulations.

The same set of simulations is repeated for a range of channel lengths and depths. The length of the channel is correlated to the widening of the channel (see Fig. 3.3a). The longer the channel, the wider the channel mouth gets. When a channel is longer, the tidal wave experiences more interaction with the bottom friction, leading to increased attenuation. To counteract this effect, the channel tends to become more convergent. The e-folding length does not follow the same pattern as b_L/b_0. The minimum e-folding length is found at a channel depth of around 20 m. Deeper channels seem to have an almost constant e-folding length independent of the channel length. Channels with $h < 20$ m have higher e-folding lengths for longer channels. This suggests that an increase in length is not 1:1 related to an increase in width of the channel mouth. The depth of the channel shows an interesting effect on the widening of the channel. At low channel depths, the widening is minimal. When the channel gets deeper the widening increases until a depth of 20 m. After that, the widening of the channel decreases again. The peak widening of a channel at a depth

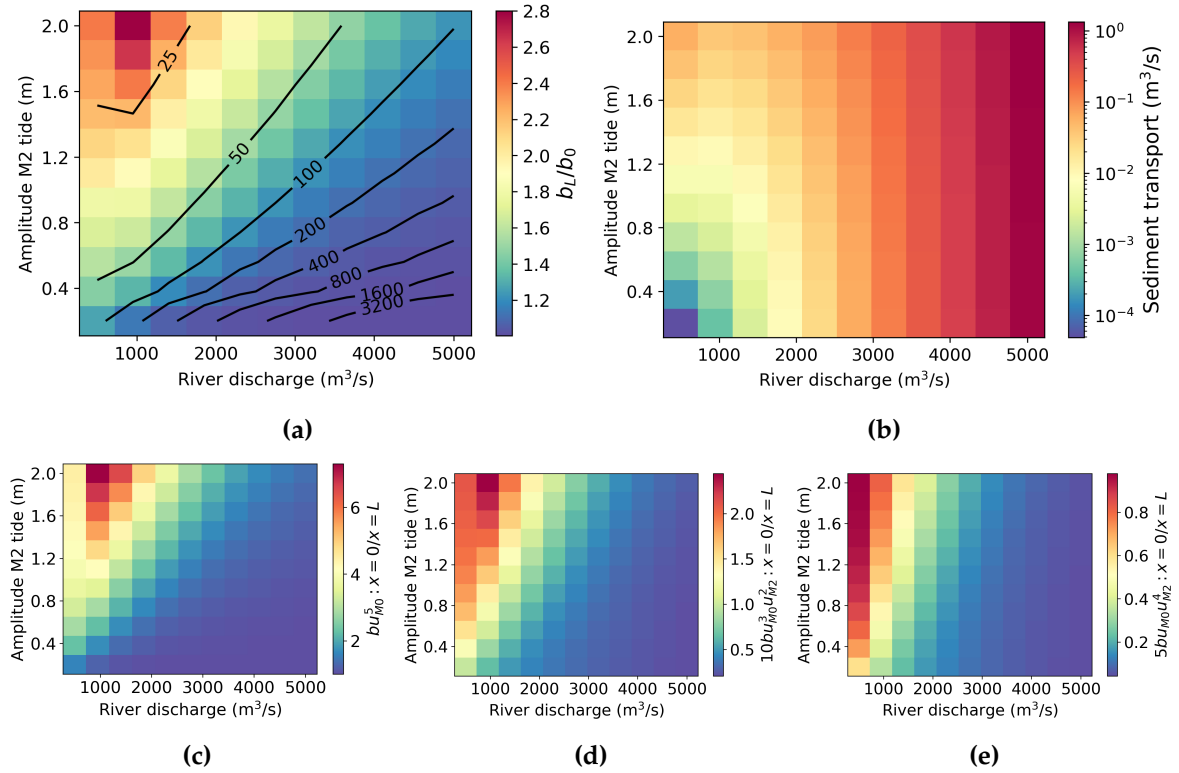

Figure 3.2: (a) Colour plot of the width ratio b_L/b_0 where b_L is the channel width at the boundary with the ocean and b_0 is the channel width at the landward boundary at morphodynamic equilibrium as a function of the river discharge and the tidal amplitude at the seaward boundary. Initially $b_L = b_0 = 300$ m, $h = 10$ m and $L = 20$ km. The upstream width, b_0, is kept fixed during the simulation. Other parameters are given in Table 2.4. The black lines show the e-folding length in km. (b) as (a) but the net sediment transport at the seaward boundary is shown in the colour plot. (c), (d) and (e) as (a) but the ratios between the different components that determine the total sediment transport $x = 0$ and $x = L$ are shown in the colour plots. The different components are $\beta b u_{M0}^5$, $10\beta b u_{M0}^3 u_{M2}^2$ and $5\beta b u_{M0} u_{M2}^4$ where $\beta = \frac{0.05}{Cd}\frac{\Theta^{2.5}}{u}\sqrt{(s-1)gd50^3}$ for (c), (d), and (e) respectively.

of 20 m is caused by the effect of the channel depth on the residual and the semi-diurnal velocities. The difference in semi-diurnal velocities at $x = L$ and $x = 0$ decreases with increasing channel dept because the bottom friction has less impact on the tidal wave. The biggest difference in net sediment transport between $x = L$ and $x = 0$ due to the semi-diurnal flow is found at low channel depths. Therefore you would assume that the least amount of widening of the channel mouth is at high depths. This is not the case because of the residual velocity which decreases with increasing channel depth causing the velocity to increase, mostly at $x = 0$, resulting in a higher net sediment transport at $x = 0$. The peak widening is found at the point where the residual velocity is low enough to not cause a big increase in net sediment transport at $x = 0$ and the semi-diurnal velocity undergoes enough damping due to friction to cause a lowering in net sediment transport at $x = 0$.

Having discussed a depth independent on time and a width dependent on time, we will proceed to study a depth dependent on time and a width independent on time. When

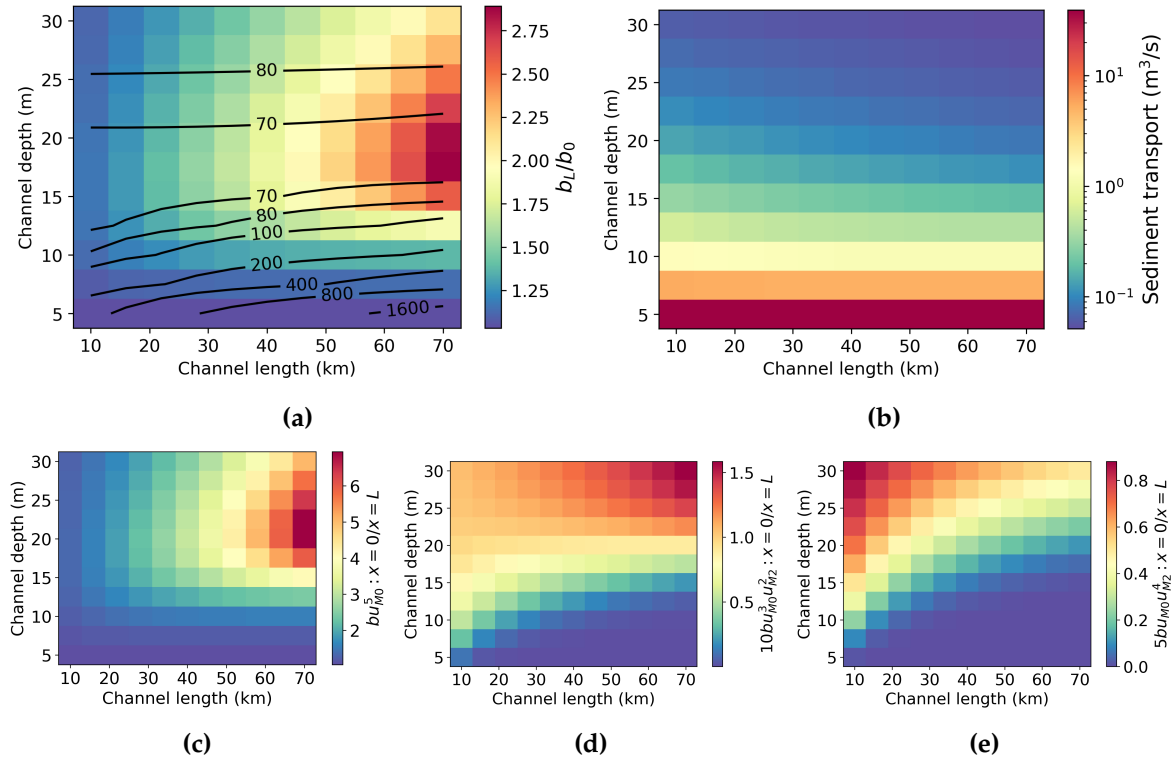

Figure 3.3: (a) Colour plot of the width ratio b_L/b_0 where b_L is the channel width at the boundary with the ocean and b_0 is the channel width at the landward boundary at morphodynamic equilibrium as a function of the channel length and the channel depth. Initially $b_L = b_0 = 300$ m. The upstream width, b_0, is kept fixed during the simulation. The discharge, $Qr = 2000$ m^3/s and the tidal amplitude, $N = 2$ m. Other parameters are given in Table 2.4. The black lines show the e-folding length in km. (b) as (a) but the net sediment transport at the seaward boundary is shown in the colour plot. (c) ,(d) and (e) as (a) but the ratios between the different components that determine the total sediment transport at $x = 0$ and $x = L$ in the colour plots. The different components are $\beta b u_{M0}^5$, $10\beta b u_{M0}^3 u_{M2}^2$ and $5\beta b u_{M0} u_{M2}^4$ where $\beta = \frac{0.05}{Cd}\frac{\Theta^{2.5}}{u}\sqrt{(s-1)gd50^3}$ for (c) ,(d) and (e) respectively.

having a prescribed e-folding length, there is not always an equilibrium depth (see Fig. 3.4a). The equilibrium channel depth increases for increasing e-folding length scales. The e-folding length scale corresponding with the depth where the channel finds an equilibrium depth for the first time is followed for different u_2/u_0, where u_2 is the maximum semi-diurnal velocity at the seaward boundary and u_0 is the residual velocity at the seaward boundary (see Fig. 3.4b). Channels with a high u_2/u_0 have a low equilibrium depth at low e-folding length scales. Having a convergent channel causes the sediment transport due to the residual flow at the seaward boundary to be lower than the sediment transport at the landward boundary leading to sedimentation (see blue line in Fig. 3.5a). This difference needs to be compensated by the sediment transport due to the semi-diurnal flow, the green and orange lines. When the erosion due to the semi-diurnal flow is not enough, the channel fills completely up, black line becomes negative. When the erosion due to the semi-diurnal flow and the sedimentation due to the residual flow find an equilibrium the net sediment

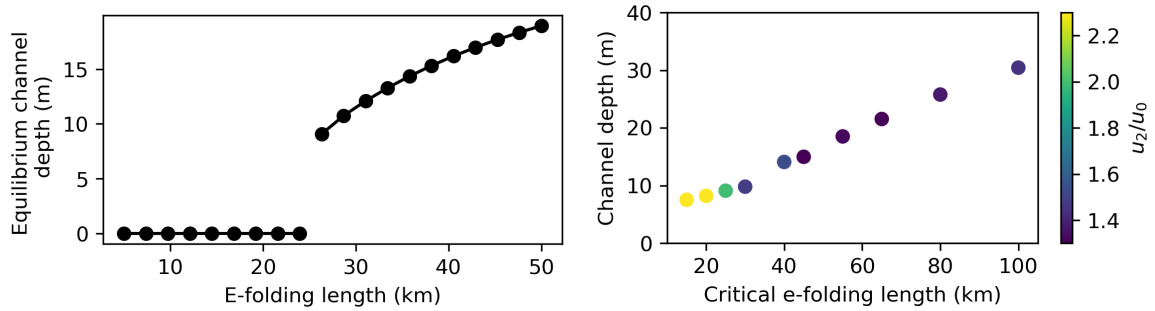

(a) **(b)**

Figure 3.4: (a) Plot of equilibrium depth or depth = 0 (closed channel) against the e-folding length scale. L = 20 km, h = 10 at the start of the simulation, b_0 = 300 m, b_L is dependent on the e-folding length, Qr = 2000 m^3/s and N = 2 m. Other parameters are given in Table 2.4. (b) The same as (a) but the critical depth, the transition between an open and closed channel, is followed for different u_2/u_0 where u_2 is the maximum semi-diurnal velocity at the seaward boundary and u_0 is the residual velocity at the seaward boundary. The colour of the doth is the strength of u_2/u_0.

transport difference between $x = 0$ and $x = L$ becomes zero (see black line in Fig. 3.5b) and the channel has gone to its equilibrium depth.

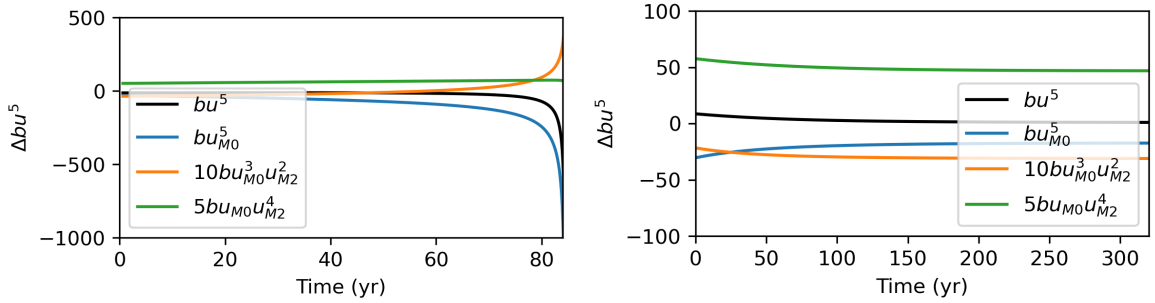

(a) **(b)**

Figure 3.5: (a) The black line shows the difference of bu^5 at x=0 and x=L over time. For the three components, the same is done. The difference in bu^5_{M0}, $10bu^3_{M0}u^2_{M2}$ and $5bu_{M0}u^4_{M2}$ at the x=0 and x=L are shown by the blue, orange and green lines respectively. In both plots initially $b_0 = 300$ m, $b_L = 450$ m, $h = 10$ m and $L = 20$ km. The width is kept fixed during the simulation and the depth is allowed to evolve. The discharge, Qr = 2000 m^3/s and the tidal amplitude, N = 2 m. Other parameters are given in Table 2.4. (b) same as (a) but $b_L = 430$ m.

3.1.3 Application to channels in nature

The width of 36 one-channel deltas from the dataset from Nienhuis et al. (2018) (see appendix C) have been modelled to test how well the model can predict the widening of channels. The depth is kept constant in time and space and can be found in the data set in appendix C. The starting widths are found in the same data set. During the simulation the widths were allowed to evolve to an equilibrium width which will be called the modelled

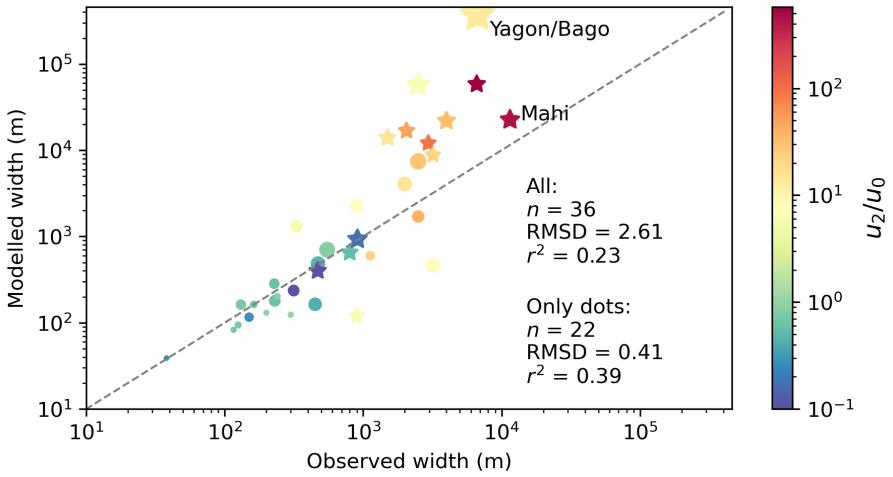

Figure 3.6: modelled width of the channel mouth against observed width of the main channels of 36 delta systems over the world. Field data are from Nienhuis et al. (2018). The colours show u_2/u_0, the maximum semi-diurnal velocity divided by the residual velocity at the seaward boundary. The size of dots and stars is relative to the channel length. When channel length is more than 10 km it is given by a star sign. RMSD is the Root Mean Square Deviation divided by the mean width (see Eq. 2.17) and r^2 is the coefficient of determination. The values of the used parameters are given in Table 2.4. The dashed grey line is the 1:1 line.

width. Shorter channels, $L < 50$ km, are modelled better than longer channels, $L > 50$ km (see Fig. 3.6). Some of the modelled widths of the longer channels are almost a factor 100 of. This creates a high RMSD of 2.61 which means that the modelled width is on average 2.61 times smaller or wider than the observed width. The channel in the data set with the largest width, 11.5 km, is that of the Mahi Delta. The channel with the largest modelled width, 509 km, is the Yangon/Bago Delta which is also the longest delta with a channel length of 208 km. The coefficient of determination, r^2, is 0.23 when looking at all deltas, meaning that 23% of the variance can be explained by the model. Looking at only the results of channels with $L < 50$ km should improve the performance of the model. The dots show the deltas that remain. The stars are all modelled widths of channels with $L > 50$ km. Both the RMSD and the r^2 improve. The RMSD went from 2.61 to 0.41 and r^2 went from 0.23 to 0.39. An r^2 of 0.39 is still low because 61% of the variance is not explained by the model. A RMSD of 0.41 means that the difference between the observed and the modelled width is on average average 41%.

The Yangon/Bago Delta is the delta with the widest modelled channel mouth. The difference in sediment transport at the landward boundary and the seaward boundary shows the first 1000 years a decrease before increasing again (see black line in Fig. 3.7b). Two mechanisms have an impact on this pattern. When the channel mouth increases in width, the cross-section area where the tides can enter the channel and the semi-diurnal velocity become bigger (see dashed orange line in Fig. 3.7c) increasing the sediment transport at the channel mouth (dashed green line in Fig. 3.7d). The convergent shape of the channel causes the tides to have a lower attenuation (solid orange line in Fig. 3.7c), which increases

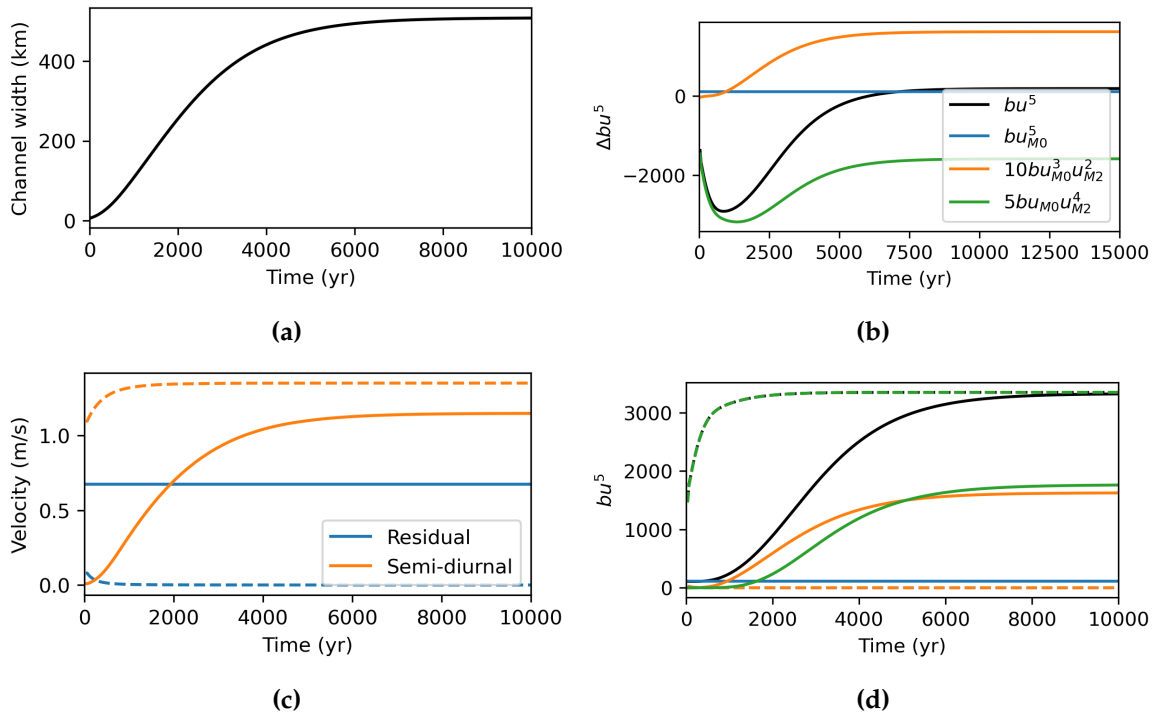

Figure 3.7: (a) Plot of the width of the channel at x=L, b_L, against time. Initially $b_0 = 800$ m, $b_L = 6694$ m, $h = 7.2$ m and $L = 280$ km. The upstream width, b_0, is kept fixed during the simulation. The discharge, $Qr = 3887$ m^3/s and the tidal amplitude, N = 2.025 m. Other parameters are given in Table 2.4. (b) shows the difference between the dashed and solid lines in panel (d). (c) as (a) but plotting the residual velocity, blue line, and the semi-diurnal velocity, orange line at $x = 0$, solid line, and at $x = L$, dashed line against time. (d) as (a) but the black line shows bu^5 at $x = 0$, solid line, and $x = L$, dashed line, over time. For the three components, the same is done. The difference in bu^5_{M0}, $10bu^3_{M0}u^2_{M2}$ and $5bu_{M0}u^4_{M2}$ at the x=0 and x=L are shown by the blue, orange and green lines respectively.

the sediment transport at the landward boundary (solid black line in Fig. 3.7d). During the first 1000 years, the increase in sediment transport at the channel mouth was faster than the increase in sediment transport at the landward boundary. After a 1000 years, the opposite was true until they found an equilibrium where both are equal.

3.2 Branching channel system

3.2.1 Sensitivity analysis

Now we have investigated how the model performs for one channel, we increase the complexity by one step and study what happens when the channel branches into two channels. First, we research the sensitivity to the forcings and starting morphology of equilibrium widths as in section 3.1.2.

The equilibrium width profiles found for the 3-channel system are very similar to the single-channel system (see Fig. 3.2a, Fig. 3.8 and Fig. 3.9). The branching of the channel

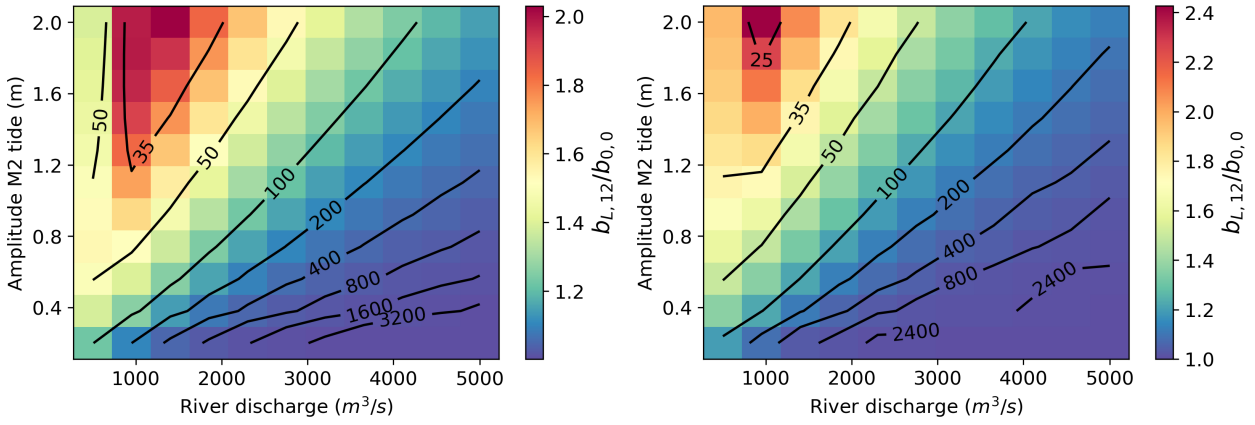

(a) **(b)**

Figure 3.8: (a) Colour plot of the width ratio $b_{L,12}/b_{0,0}$ where $b_{L,12}$ is the sum of the channel widths at the boundary with the ocean and $b_{0,0}$ is the channel width of channel 0 at the landward boundary at morphodynamic equilibrium as a function of the river discharge and the tidal amplitude at the seaward boundary. Initially $b_L = b_0 = 300$ m for channel 0 and $b_L = b_0 = 150$ m for channels 1 and 2, $h = 10$ m and $L = 10$ km. The upstream width, b_0, is kept fixed during the simulation. Other parameters are given in Table 2.4. The black lines show the e-folding length in km. (b) as (a) but b_0 is not kept constant but calculated using Equation 2.18.

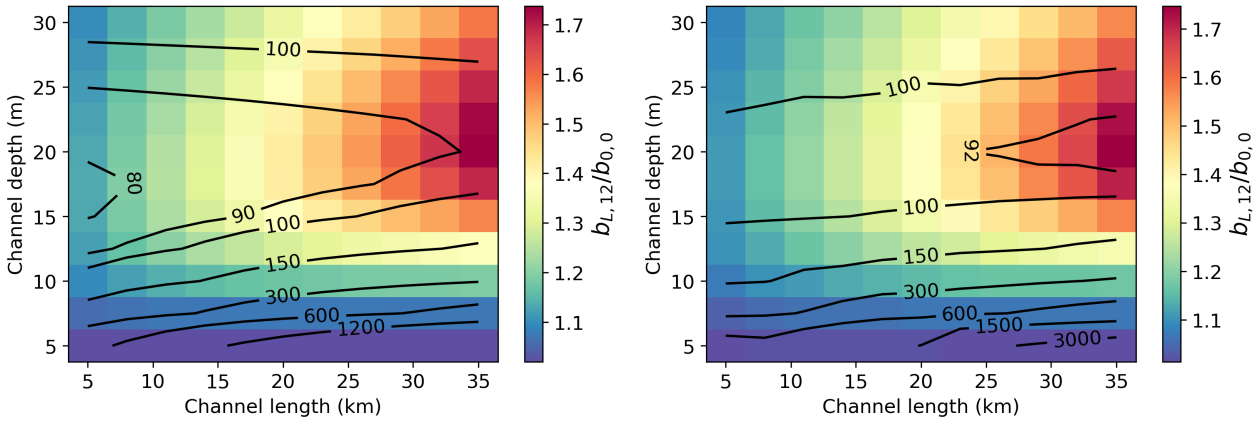

(a) **(b)**

Figure 3.9: (a) Colour plot of the width ratio $b_{L,12}/b_{0,0}$ where $b_{L,12}$ is the sum of the channel widths at the boundary with the ocean and $b_{0,0}$ is the channel width of channel 0 at the landward boundary at morphodynamic equilibrium as a function of the channel length and the channel depth. Initially $b_L = b_0 = 300$ m for channel 0 and $b_L = b_0 = 150$ m for channels 1 and 2, $Qr = 2000$ m^3/s and $N = 2$ m. The upstream width, b_0 is kept fixed during the simulation. Other parameters are given in Table 2.4. The black lines show the e-folding length in km. (b) as (a) but b_0 is not kept constant but calculated using Equation 2.18.

causes the sum of the channel mouths to be lower. Keeping the upstream widths constant of channels 1 and 2 causes the channel to widen less compared to letting them evolve so that $b_{0,L} = b_{1,0} + b_{2,0}$. This is most profound at low discharges and high tidal amplitudes. The dependence of the channel width on the channel depth is still the same where the channel

width increases for an increasing channel depth till a maximum at around $h = 20$ m whereafter the width decreases again for increasing depth (see Fig. 3.9). The dependence on the channel length changes slightly, most clearly visible when looking at the e-folding lengths (black lines in Fig. 3.9). The single-channel system (Fig. 3.3a) and the branching channel system keeping the upstream widths constant (3.9a) have a similar pattern. When letting the upstream widths of channel 1 and 2 evolve the pattern at $h < 15$ m are similar but for deeper channels the dependence on the channel length is mirrored.

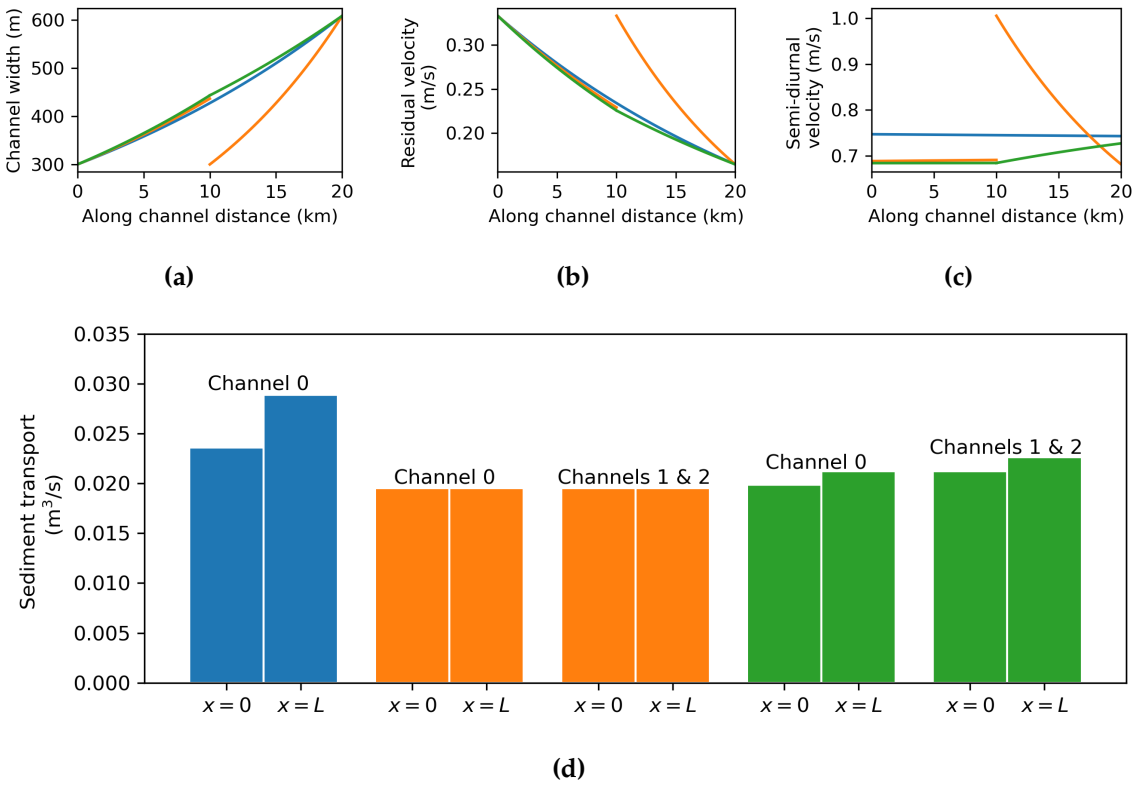

Figure 3.10: (a) Plot of channel width against the along channel distance. The widths of channels 1 and 2 are added together. The blue line shows the width of the one-channel system, the orange line shows the width of the branching channel system with a constant b_0 and the green line shows the width of a branching channel system where the upstream width of channels 1 and 2 are dependent on there sediment transport. For the one-channel system, $b_0 = 300$ m, $b_L = 608$ m, $h = 10$ m and $L = 20$ km. For the branching channel system with br=constant, $b_0 = 300$ m and $b_L = 436$ m for channel 0 and $b_0 = 150$ m and $b_L = 304$ m for channels 1 and 2, $h = 10$ m and $L = 10$ km. For the branching channel system with br is not constant, $b_0 = 300$ m and $b_L = 443$ m for channel 0 and $b_0 = 222$ m and $b_L = 304$ m for channels 1 and 2, $h = 10$ m and $L = 10$ km. For all, $Qr = 1000$ m^3/s and $N = 2$ m. Other parameters are given in Table 2.4. (b) as (a) but the residual velocity is plotted against the along-channel distance. (c) as (a) but the semi-diurnal velocity is plotted against the along-channel distance. (d) as (a) but the sediment transport is plotted in a bar plot for each channel at the start and at the end.

To investigate the difference between the one-channel system, the branching channel system with constant upstream width and the branching system with evolving upstream width, all were allowed to evolve in width until one of the systems reached their equilibrium

width. The branching channel with a constant upstream width found its equilibrium width fastest. All simulations were stopped having the same width of 608 m at $x = 20$ km. For the branching channels, the downstream widths were added together. The width profile (Fig. 3.10a) and the residual velocity (Fig. 3.10b) of the single-channel, the blue lines, and the branching channel system with an evolving upstream width, the green lines, are very similar but the semi-diurnal velocities do show a different pattern (see Fig. 3.10c). The semi-diurnal velocity of the single channel is higher, resulting in higher sediment transports (see Fig. 3.10d). Both systems are not in equilibrium because the sediment transport at the seaward boundaries is higher than the sediment transport at the riverward boundary. The branching channel system with constant upstream width is in equilibrium as the sediment transport at all boundaries is equal. The main difference with the other systems is the lower semi-diurnal velocity of channels 1 and 2 at the seaward boundary ($x = 20$ km) resulting in a lower sediment transport equal to the sediment transport at the riverward boundary ($x = 10$ km).

3.2.2 Stability of found equilibrium widths

Having found the equilibrium widths, their stability is tested by performing a perturbation. If the depth is perturbed and is allowed to evolve there are three possible end scenarios. The first possibility is that the depth goes back to its old depth (see Fig. 3.11a). The second possibility is that the depth goes to a different depth (see Fig. 3.11b) and the last option is that one of the downstream channels completely closes off. The deeper channel gets extra sediment transport due to transverse sediment transport (see Fig. 3.11c). If this is more than the extra sediment transport caused by the higher velocity due to the channel being deeper then the sediment transport at $x = 0$ is higher, than the sediment transport at $x = L$ and the channels will go back to an symmetrical equilibrium. If the transverse sediment transport is not higher than the extra sediment transport at $x = L$ due to the higher velocities the channel will become deeper until an equilibrium is found or one of the channels completely closes.

This experiment is repeated for different discharges but also for different tidal amplitudes resulting in Figure 3.12a. When looking at N = 0.5 m, you can see that the system goes back to the symmetrical geometry after being perturbed till a discharge of approximately 1100 m^3/s. For higher discharges the system finds new equilibrium depths causing the discharge asymmetry between the downstream channels, $\Psi_Q = \frac{Q_1 - Q_2}{Q_0}$, to not longer be zero. The moment when the discharge asymmetry between the downstream channels is no longer zero is called the bifurcation point. Having tides moves the bifurcation point to higher discharges. When the two downstream channels are symmetrical but one of the channels is slightly deeper, the amplitude of the semi-diurnal velocity at the seaward boundary is lower in the deeper channel. This causes a relatively low net sediment transport at the seaward boundary. Which in turn lowers the bed level difference between the two channels causing the channels to be symmetrically stable for higher discharges. After the bifurcation point, the discharge asymmetry between the two downstream channels first increases for

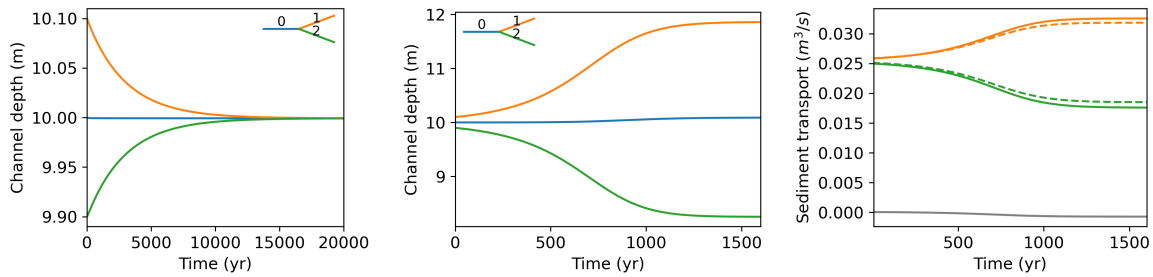

(a) (b) (c)

Figure 3.11: (a) Plot of the channel depth over time. Channel 0 is shown by the blue line, channel 1 is the orange line and channel 2 is the green line. For channel 0 $b_L = b_0 = 300$ m and $b_L = b_0 = 150$ m for channels 1 and 2 and $L = 10$ km, $h = 10$ m for channel 0, 10.1 m for channel 1 and 9.9 m for channel 2. The tidal amplitude, $N = 0.5$ m and the discharge, $Qr = 1000$. Other parameters are given in Table 2.4. (b) as (a) but $Qr = 2000$. (c) as (b) but the sediment transport at the junction is plotted. The orange lines are the sediment transport that channel 1 receives, the green line are the sediment transport that channel 2 receives and the grey lines are the transverse sediment transport upstream of the channel where positive is from channel 1 to channel 2. The dashed lines are the sediment transport without the transverse sediment transport.

increasing discharge before decreasing again. This means that larger tidal amplitudes can have a larger discharge asymmetry than a lower tidal amplitude for certain river discharges. At a discharge of 4500 m^3/s, $N = 0.5$ has almost the same discharge asymmetry as the case without any influence of tides.

In Figure 3.12a the upstream width was kept constant while in Figure 3.12b the upstream width was allowed to evolve depending on the received sediment transport. Allowing the upstream width to evolve keeps the stable equilibrium solution of the channel network longer symmetrical.

In Figures 3.12c, 3.12d, 3.12e and 3.12f the width or depth is perturbed and after that, the width was allowed to go to an equilibrium. No matter if the perturbation was in the depth or width, and whether the upstream width was kept constant or not, all went back to an almost symmetrical equilibrium independent of the strength of the tides resulting in a discharge asymmetry close to zero. The stabilising effect of a width that is allowed to change in time has to do with the way the width and depth are related to the velocity. To keep the explanation as simple as possible, we will look at a branching channel with a constant width and only the river discharge as forcing. At the start, both channels have the same width and channel 1 is slightly deeper than channel 2. The velocity is given by Equation 2.7: $u = -\frac{gh}{\lambda}\frac{d\eta}{dx}$. At the junction and the boundaries with the ocean, the free surface elevation of both downstream channels needs to be equal to each other as prescribed in the boundary conditions. Therefore $\frac{\partial \eta_1}{\partial x_1} = \frac{\partial \eta_2}{\partial x_2}$. Consequently the velocities in both channels do not depend on the width but only on the depth. The system found an equilibrium when in all channels the incoming sediment transport is equal to the outgoing sediment transport. The incoming sediment transport of the two downstream channels is defined by Equation 2.11. The sediment transport is equally spread between the two downstream

channels plus an extra sediment flow to the deeper channel, Qsy. The outgoing sediment transport is defined by Equation 2.10, where $Qs \propto u^5 \propto h^5$. For channel 1 to be in equilibrium, $Qsy = \frac{h_1^5}{h_1^5+h_2^5} Qs_0 - \frac{1}{2} Qs_0$ but Qsy is also dependent on the depth difference between the two downstream channels. At higher river discharges, the depth difference between channels 1 and 2 has to be relatively large before $Qsy = \frac{h_1^5}{h_1^5+h_2^5} - \frac{1}{2} Qs_0$. This is what happens the depth is allowed to evolve and the width is kept constant in time and space. Now the width is allowed to evolve and the depth is kept constant. The upstream width is kept constant while the downstream width is allowed to change. The deeper channel needs to widen slightly to compensate for the extra sediment transport due to the higher velocity and Qsy. Channel 2 does the opposite, the width at the seaward boundary will decrease slightly in comparison with the width at the junction. The widening of the channels is minimal causing $Q_1 \approx Q_2$.

The discharge asymmetry is never equal to zero for a channel system which is perturbed in the width and has an evolving depth (see Fig. 3.12g and 3.12h). This is because the width

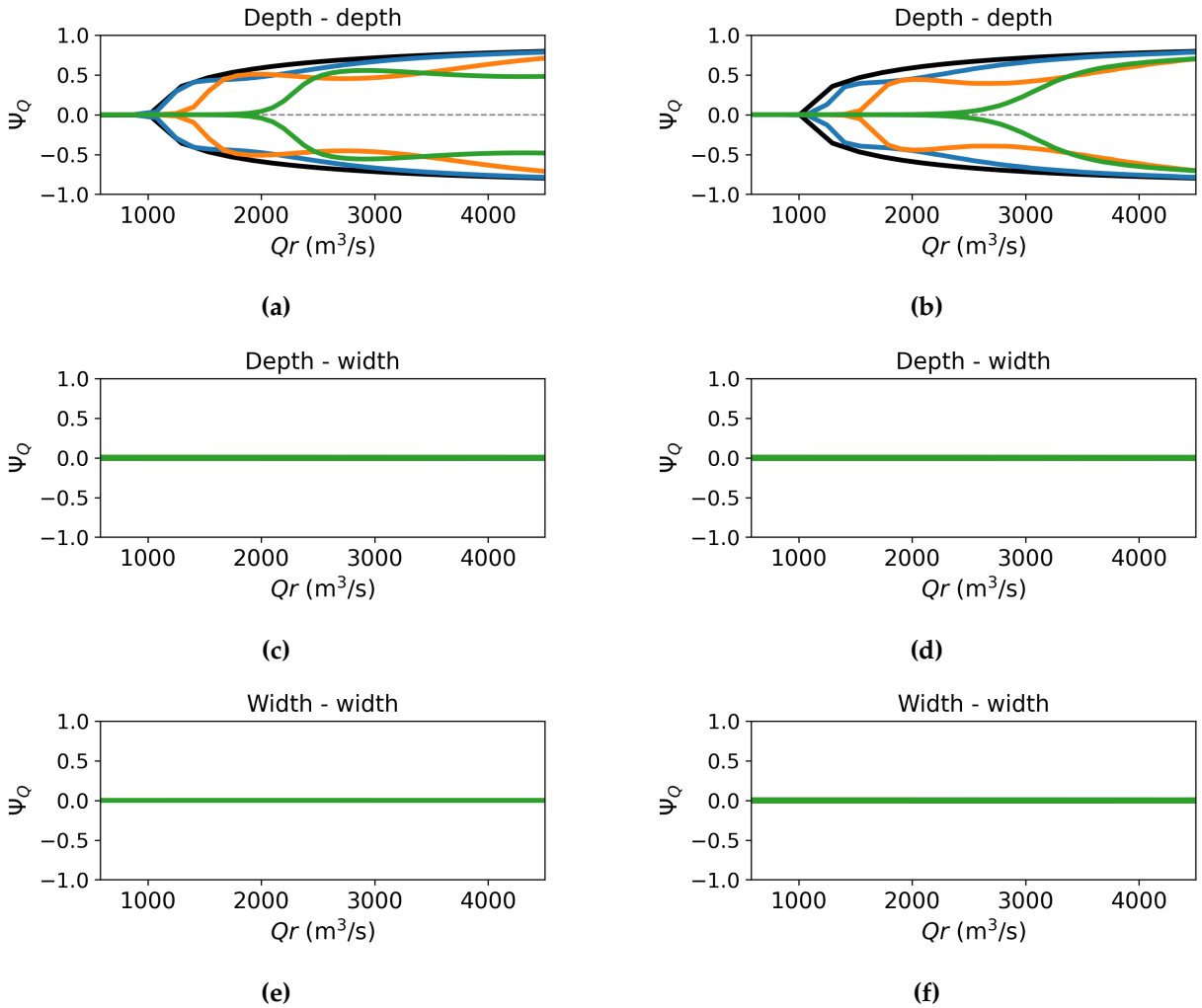

Figure 3.12

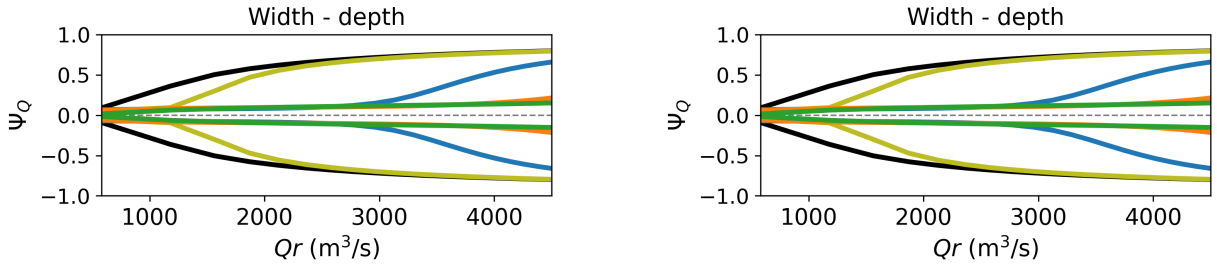

(g) **(h)**

Figure 3.12: (continued) The discharge asymmetry against the prescribed discharge is plotted. The black line shows the results of N = 0 m, the yellow lines the results of N = 0.1 m, the blue line the results of N = 0.5 m, the orange line the results of N = 1 m and the green line the results of N = 2 m. The dotted grey line is the unstable symmetrical solution. The discharge asymmetry is calculated by $\Psi_Q = \frac{Q_1 - Q_2}{Q_0}$ where the subscribe refers to the channel index and Q to the tidally averaged discharge. The title of the plot says first if the width/depth is perturbed and then if the width/depth was allowed to evolve to an equilibrium. The used parameters are given in Table 2.4 and the starting dimensions in Table 2.5. The upstream width of the two downstream channels is kept constant in (a), (c), (e) and (g). The upstream width of the two downstream channels is allowed to vary depending on the sediment transport in (b), (d), (f) and (h). The dotted grey line are the unstable symmetrical equilibrium solutions.

and the depth are not in the same way related to the sediment and discharge distribution. The strength of the tides have a strong impact on the results. The stronger the tides, the longer the channel network stays close to being symmetrical for increasing discharge. The results are very similar for the case where the upstream width was kept constant, Figure 3.12g, and for the case where the upstream width was allowed to evolve, Figure 3.12h.

3.2.3 Application to a branching channel in the Mekong Delta

A branching channel in the Mekong Delta is researched to compare model results with observations. First, the channels were allowed to go to an equilibrium width. The upstream widths of the channels were kept constant in time. After that, the depth was perturbed and allowed to evolve. This was done for a discharge ranging between 1200 and 16000 m^3/s and tidal amplitudes of 0, 0.1, 0.5 and 1.3 m.

The results of the stability of a branching channel in the Mekong (see Fig. 3.13) are comparable with results in Figure 3.12a. The Shields stress corresponding with the tested discharges ranges between 0.002 and 0.323 for the simulations without tidal forcing in the Mekong Delta. In Figure 3.12a the Shields stress for the simulation without tidal forcing ranges between 0.005 and 3.

The discharge asymmetry calculated by Eslami et al. (2019) (see red dot in Fig. 3.13) is higher than the discharge asymmetry calculated by the model. Channels 1 and 2 were assumed to be symmetrical. Channel 1 is actually wider than channel 2 as seen in Figure 2.6. Therefore the same simulations are repeated but the starting width of channel 1 is larger than

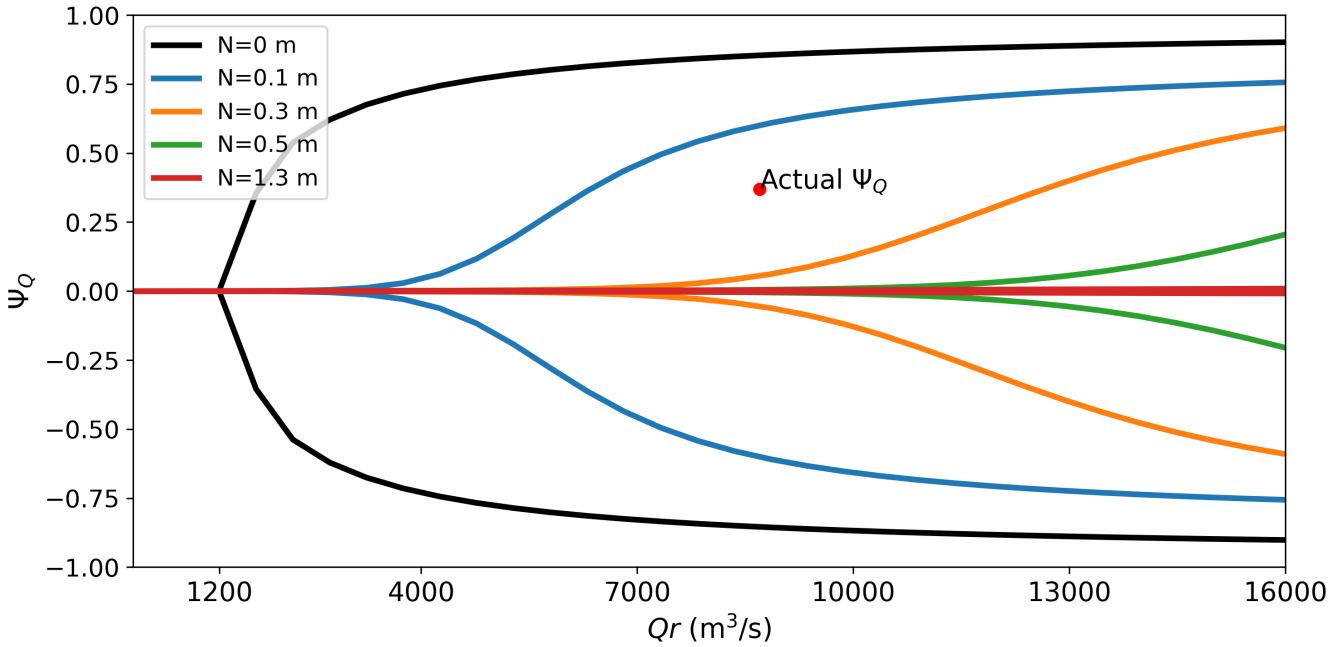

Figure 3.13: Bifurcation diagram of branching channel in the Mekong Delta. The discharge asymmetry is plotted against the discharge. The black line is the result for the simulation without tides, the blue line for the simulation with 0.1 m tidal amplitude, the orange line for 0.3 m, the green line for 0.5 m and the red line for 1.3 m. The red dot shows the discharge asymmetry calculated by Eslami et al. (2019). Values of the used parameters in table 2.4 and the starting dimensions in tables 2.6.

the starting width of channel 2 (see Tab. 3.1). Now the modelled discharge asymmetry is closer to the discharge asymmetry calculated by Eslami et al. (2019) (see Fig. 3.14). Because the upstream widths are kept constant, the channel system is not able to become symmetrical again resulting in a discharge asymmetry which is always larger than zero.

	Channel 0	Channel 1	Channel 2
Channel length	33 km	33 km	33 km
Channel depth	11.2 m	11.2 m	11.2 m
Channel width	2900 m	1750 m	1150 m

Table 3.1: Dimensions of part of Mekong Delta.

3.3 Branching channel network with connecting channel without tides

3.3.1 Stability of branching channel network with connecting channel

To next step is adding a connecting channel between the two downstream channels. Because this is not done before, the influence of tides is removed to keep the system as simple

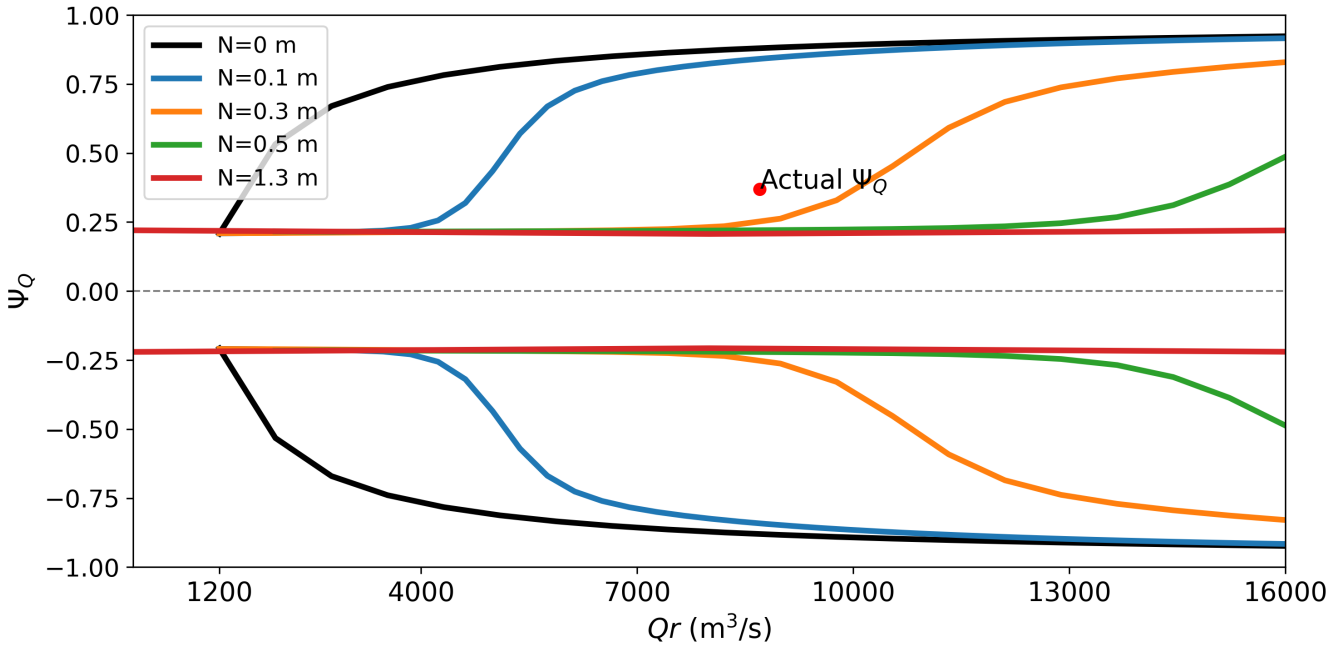

Figure 3.14: Bifurcation diagram of branching channel in the Mekong Delta. The discharge asymmetry is plotted against the discharge. The black line is the result for the simulation without tides, the blue line for the simulation with 0.1 m tidal amplitude, the orange line for 0.3 m, the green line for 0.5 m and the red line for 1.3 m. The red dot shows the discharge asymmetry calculated by Eslami et al. (2019). Values of the used parameters in table 2.4 and the starting dimensions in tables 3.1.

as possible. Having tides added the need for a converging channel. Now without any tidal forcing, the channels can have a constant width and still find an equilibrium solution. Therefore only the depth evolution of the network is researched. The starting situation is a symmetrical branching channel with a connecting channel added. The channel depth of the downstream channels were perturbed and after that all channel depths were allowed to evolve. This is done for a range of river discharges which can be rewritten as a Shields stress (see Eq. 2.10a). This resulted is two different states. A non-periodic state (Fig. 3.15a) and a periodic state (Fig. 3.15b). In the non-periodic state, the channel depths all evolve to an equilibrium depth and stay there as long as the forcings do not change. In the periodic state, the channels 1 and 2 and channels 4 and 5 switch between being the deeper and the shallower channel.

To understand what happens during the periodic behaviour, a smaller time period is shown in Figure 3.16. 70 years in the simulation, channel 4 is deeper than channel 5 (see Fig. 3.16a). Channel 4 increases in depth until 79 years (see purple line in Fig. 3.16a) at the same time channel 5 becomes more shallow (see brown line in Fig. 3.16a). This causes a decrease in difference between the free surface elevation at $x = 0$ of channels 4 and 5 until the free surface elevation of both channels is equal (see Fig. 3.16b). The moment the free surface elevation between the two channels is zero, the velocity in channel 3 switched direction (see red line in Fig. 3.16c). Because of this, the junction between channels 1, 3 and 4

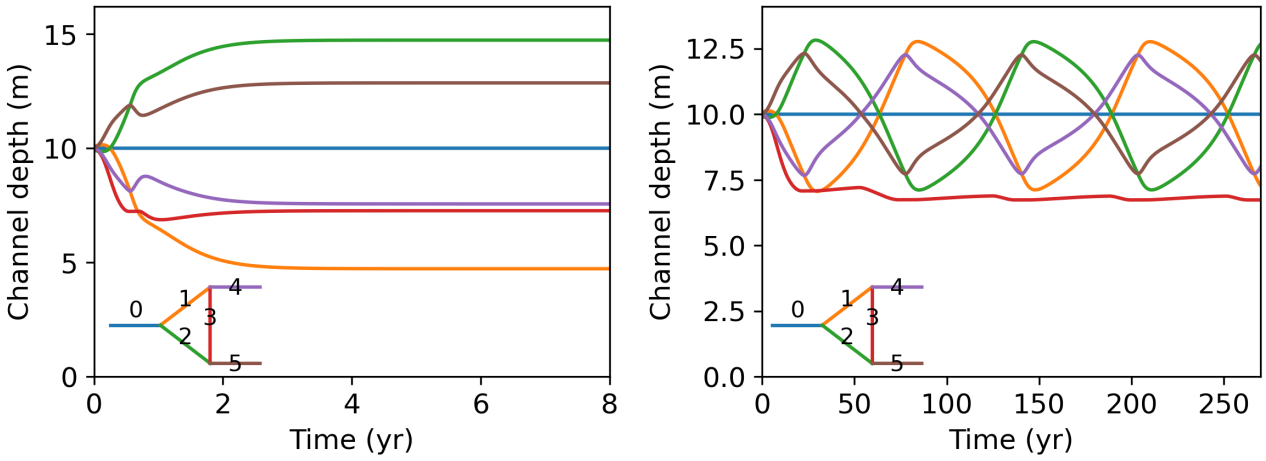

Figure 3.15: (a) Plot of the channel depth over time. The blue line is the depth of channel 0, the orange line is the depth of channel 1, the green line is the depth of channel 2, the red line is the depth of channel 3, the purple line is the depth of channel 4 and the brown line is the depth of channel 5. The starting dimensions are given in Table 2.8. The discharge, Qr = 2000 m^3/s and the other parameters are given in table 2.4. (b) as (a) but Qr = 4000 m^3/s.

becomes a branching point instead of a confluence (see solid purple line in Fig. 3.16d). Even though channel 4 receives no sediment transport from channel 3 anymore, the sediment transport entering channel still increases due to the increase in velocity in channel 1 (see orange line in Fig. 3.16c). Resulting in a higher sediment transport at $x = 0$ than at $x = L$, so sedimentation. In channel 5 the opposite happens. This process repeats itself resulting in periodic behaviour.

Without connecting channel the system is symmetrically stable till a Shields stress of 0.17 (see Fig. 3.17). For higher Shields stresses the system becomes asymmetrical after being perturbed and allowed to change its channel depths resulting in a discharge asymmetry not equal to zero. Adding the connecting channel allows the network to go into a stable periodic solution for a range of Shields stresses. The discharge asymmetry when being in a periodic state can be anywhere between the dotted lines depending on the time. The periodic behaviour starts at a Shields stress of 0.41 and ends at a Shields stress of 1.43. The discharge asymmetry between channels 1 and 2, Ψ_{Q12}, and the discharge asymmetry between channels 4 and 5, Ψ_{Q45}, are not equal to each other. Before the periodic solution, Ψ_{Q45} is bigger than Ψ_{Q12}. During the periodic solution and after the opposite is true. The discharge asymmetry between channels 1 and 2, Ψ_{Q12}, is always closer to the stable solution of the channel network without connecting the channel than the discharge asymmetry between channels 4 and 5, Ψ_{Q45}.

At the start of the simulation, after the perturbation, both the system with and without connecting channel have exactly the same discharge distribution because $\frac{d\eta}{dx} = 0$ for channel 3 meaning that the free surface elevation at the junctions connected to channel 3 are equal to each other (see Fig. 3.18a) So why do they evolve differently? In the system with the

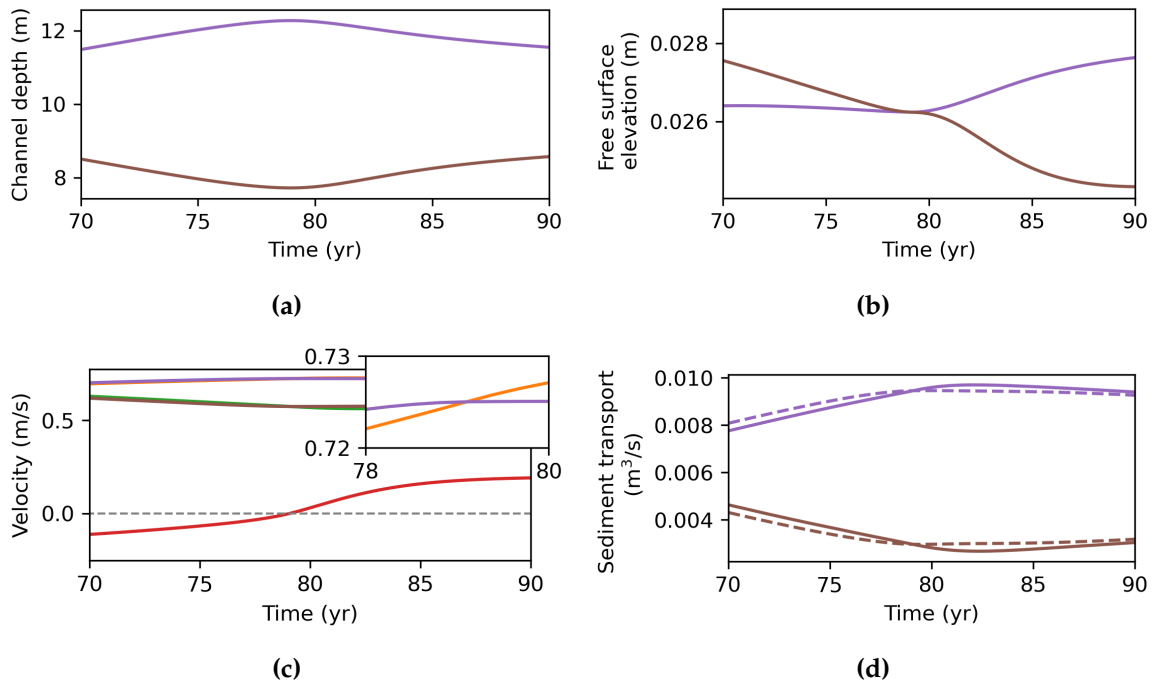

Figure 3.16: (a) As Fig. 3.15 but for period between 70 and 90 years. (b) as (a) but the free surface elevation at $x = 0$ is plotted against time. (c) as (a) but velocity plotted against time. The orange line shows the velocity of channel 1, the green line the velocity of channel 2 and the red line the velocity of channel 3 where a positive value means a flow from channel 4 towards channel 5 and a negative value a flow from channel 5 towards channel 4. The dashed grey line shows a velocity of zero. (d) as (a) but sediment transport plotted against time. Solid line is the sediment transport at $x = 0$ and the dotted line is the sediment transport at $x = L$.

connecting channel, only channels 1 and 2 change depth during the first time step because the incoming and outgoing sediment transport of the other channels is only dependent on the velocity which is equal at both channel ends. After the first time step channels 1 and 4 and channels 2 and 5 do not have the same depth anymore causing $\frac{d\eta_1}{dx} \neq \frac{d\eta_2}{dx}$ and $\frac{d\eta_4}{dx} \neq \frac{d\eta_5}{dx}$ resulting in a flow through the connecting channel (see Fig. 3.18b). This increases the final discharge asymmetry at low Shields stresses and decreases the final discharge asymmetry at high Shields stresses.

Using the method described in section 2.4.1, the model found only the stable non-periodic and periodic solutions. To also find the unstable solutions the stable solutions were followed by adding or subtracting 5 m^3/s to the river discharge every 200 time steps.

Plotting the stable and unstable solutions in one plot shows that the non-periodic solutions originate from two pitchfork bifurcations (see Fig. 3.19). In a pitchfork bifurcation, the stable symmetrical solution splits up into two stable asymmetrical solutions. Following the stable solution at low Shields stresses showed that the unstable solution, the blue dashed lines, moves towards the stable solution of the channel network without the connecting channel, the black lines, but never reaches it completely. When following the periodic state, the blue pluses, to higher Shields stresses they kept existing. Periodic behaviour

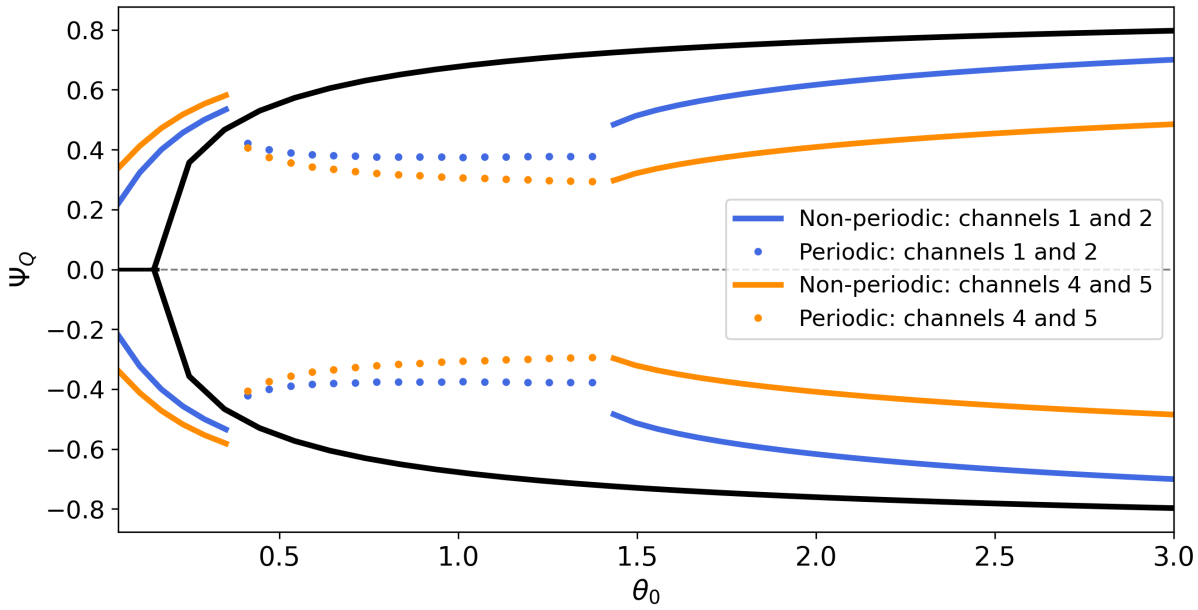

Figure 3.17: Bifurcation diagram of branching river with connecting channel. The discharge asymmetry is plotted against the Shields stress of channel 0. Values of the used parameters in Table 2.4 and the starting dimensions in Tables 2.8 and 2.7 option 1. The orange lines show the solutions of channels 1 and 2 and the blue lines show the solutions of channels 4 and 5. The solid lines are the non-periodic solutions and the dotted lines show the periodic solutions. The discharge asymmetry can be anywhere between the two dotted lines. The black line shows the discharge asymmetry of the channel network without the connecting channel and the dashed grey line is the unstable symmetrical solution for both the channel network with and without the connecting channel.

normally originates from a Hopf bifurcation. In a Hopf bifurcation, the symmetrical stable solution becomes unstable and stable periodic solutions arise after a critical point. Therefore it would be logical if the periodic behaviour originates from a sub-critical Hopf bifurcation at a Shields stress higher than the researched range.

Adding the connecting channel allowed periodic behaviour to form for a range of Shields stresses. To learn more about the periodic behaviour, the period and amplitude were analysed. The model was run for at least twenty periods to receive enough data to analyse the trend in period and amplitude for 20 different Shields stresses. The peaks were located by finding the highest channel depth at each periodic cycle. The period was calculated by calculating the time between each peak and the amplitude by taking the maximum depth minus the average depth of that channel while being in a periodic state. Both the amplitude and the period decreases for increasing Shields stresses. The dependence of the amplitude on the Shields stress is also visible in the decreasing trend in the discharge asymmetry between the two downstream channels in Figure 3.17. An increasing Shields stress correspondents with an increase in river discharge, leading to higher velocities. These higher velocities enhance sediment transport, which in turn speeds up morphological changes and reduces the

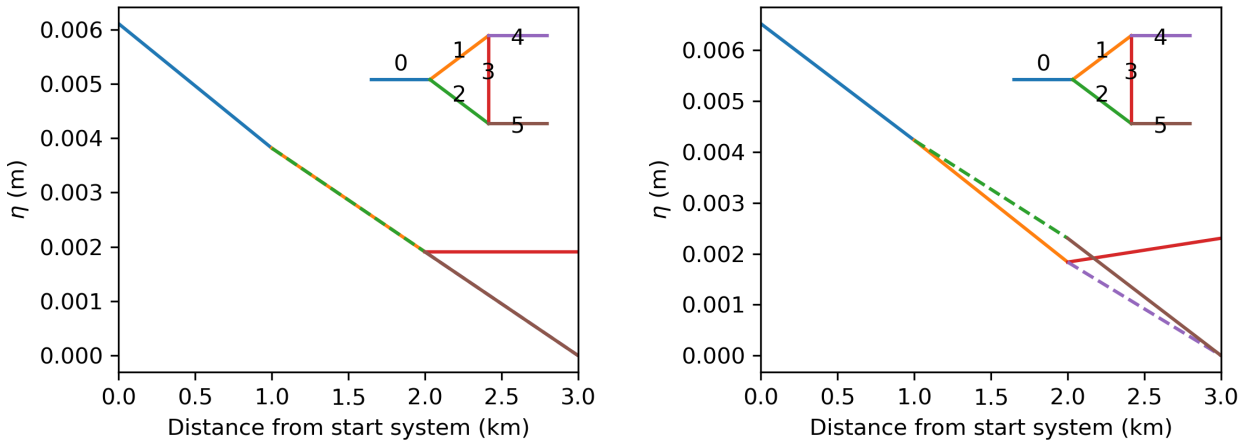

(a) **(b)**

Figure 3.18: (a) Plot of the free surface elevation along the channel system. The blue line is the depth of channel 0, the orange line is the depth of channel 1, the green line is the depth of channel 2, the red line is the depth of channel 3, the purple line is the depth of channel 4 and the brown line is the depth of channel 5. The starting dimensions are given in Table 2.8 but the depths of channels 1 and 4 are 15 m and of channels 2 and 5 are 5 m. The discharge, Qr = 2000 m^3/s and the other parameters are given in table 2.4. (b) as (a) but the depth of channel 1 is 12 m and of channel 2 = 8 m.

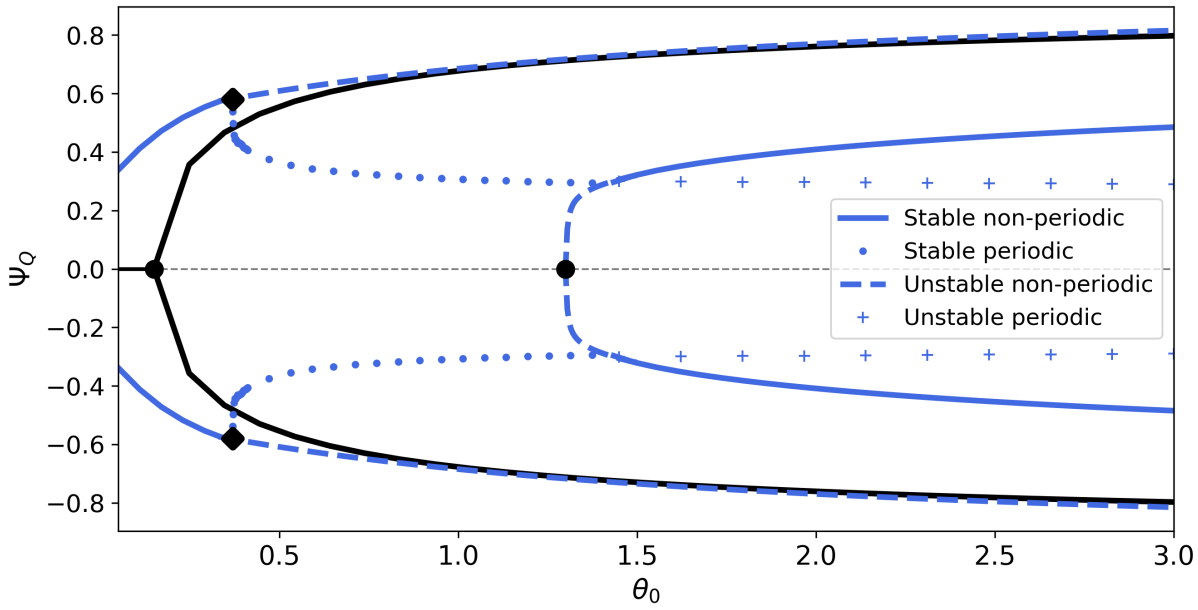

Figure 3.19: Same as Figure 3.17 but with unstable solutions given by the dashed lines for the non-periodic solutions and the pluses for the periodic solutions. The discharge asymmetry is only given between channels 4 and 5. The black dots denote a pitchfork bifurcation and the diamonds that the periodic solution is being absorbed by the non-periodic solution.

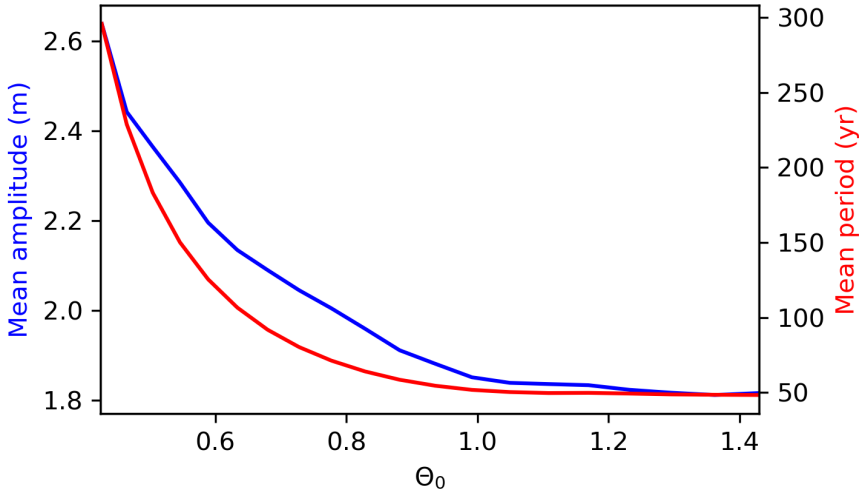

Figure 3.20: The amplitude, blue line, and the period, red line, of the periodic behaviour plotted for different Shields stresses. The Shields stress is calculated in channel 0. Values of the used parameters in Table 2.4 and the starting dimensions in Tables 2.8 and 2.7 option 1.

period.

3.3.2 Impact width of the connecting channel on equilibrium solutions

Decreasing the width of the connecting channel changes the discharge asymmetry between the downstream channels of the stable equilibrium solution (see Fig. 3.21). The range of Shields stresses with periodic behaviour becomes smaller and lower having a smaller connecting channel. The discharge asymmetry of the stable non-periodic equilibrium solutions moves closer to the discharge asymmetry of a channel network without a connecting channel. Having a connecting channel with a width of ten meters, the non-periodic stable solutions almost overlap with the stable solutions of the channel network without a connecting channel but still has a range of Shields stresses where the stable solutions are periodic.

3.3.3 Application to the Wax Lake Delta

The Wax Lake Delta is a delta with multiple connecting channels. With the current dimensions, the model calculated that 88% of the discharge goes to channel 1 and 12% to channel 2, which corresponds with $\Psi_{Q12} = 0.76$. This should be 92% to channel 1 and 8% to channel 2 (Meselhe et al., 2021). Downstream of the connecting channel, the modelled discharge is slightly less unevenly spread over channels 4 and 5, with channel 4 getting 87% of the discharge and Channel 5 13%, $\Psi_{Q45} = 0.75$. These percentages are the same as given in Meselhe et al. (2021). Letting the channel depth evolve results in a deepening of channels 2 and 5. Which causes the discharge in channels 2 and 5 to be higher than in channels 1 and 4 (see Fig. 3.22). The discharge asymmetry between the downstream channels increases for increasing Shields stress. Adding the connecting channel lowers the discharge asymmetry

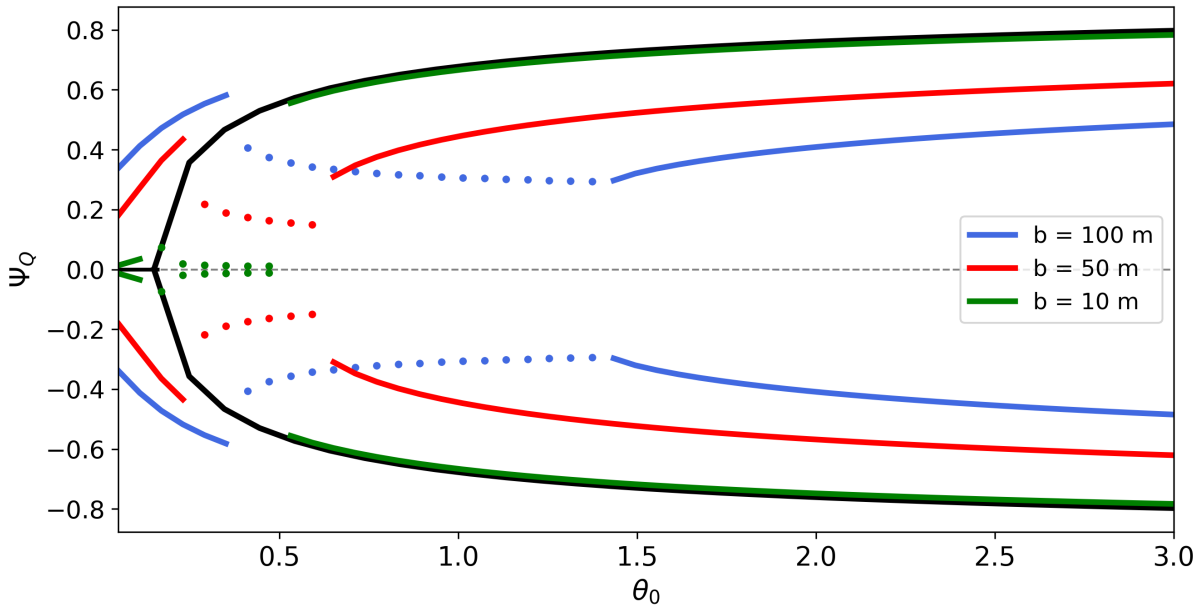

Figure 3.21: Bifurcation diagram with different widths of the connecting channel. The discharge asymmetry between channels 4 and 5 is plotted against the Shields stress. The blue lines have a connecting channel with a width of 100 m. The red lines have a connecting channel with a width of 50 m. The green lines have a width of 10 m. The non-periodic solution is given by the dotted lines and the periodic solution is given by the solid lines. The black lines give the discharge asymmetry of the channel network without connecting the channel. Values of the used parameters in table 2.4 and the starting dimensions in tables 2.8 and 2.7 option 1.

between channels 1 and 2 and increases the discharge asymmetry for channels 4 and 5.

Looking at how the system changes over time with a $Qr = 2520$ m^3/s shows that there are two time periods, from 0 years til 30 years and from 100 til 200 years, when the system changes the most (see Fig. 3.23b). At the start of the simulation channels 4 and 5 (the purple and brown line) become shallower indicating that the sediment transported received upstream is higher than the sediment leaving the channel downstream (see Fig. 3.23d and Fig. 3.23e). This is because channels 4 and 5 are wider than channels 1 and 2 respectively causing the velocity in channels 4 and 5 to be lower (see Fig. 3.23c). Channel 3 has a relative low velocity (the red line) together with being shallow and narrow, the flow has a relative small impact on the other channels at the start of the simulation. The velocity in channel 3 till 20 years is negative, meaning that the flow is directed towards channels 1 and 4. This together with becoming more shallow creates a peak in the channel velocity of channel 4. 20 years into the simulation channels 1 and 4 become more shallow resulting in a higher discharge in channels 2 and 3 and therefore higher velocities increasing the sediment transport (see Fig. 3.23f). After 30 years the system seems to stabilise but channel 3 slowly deepens. 150 years into the simulation channel 3 transports almost enough sediment from channel 1 to channel 5 to to stop the deepening of channel 5 and the shallowing of channel 4 (see Fig. 3.23b and Fig. 3.23g). The sediment transport at $x = 0$ and $x = L$ is always equal, therefore

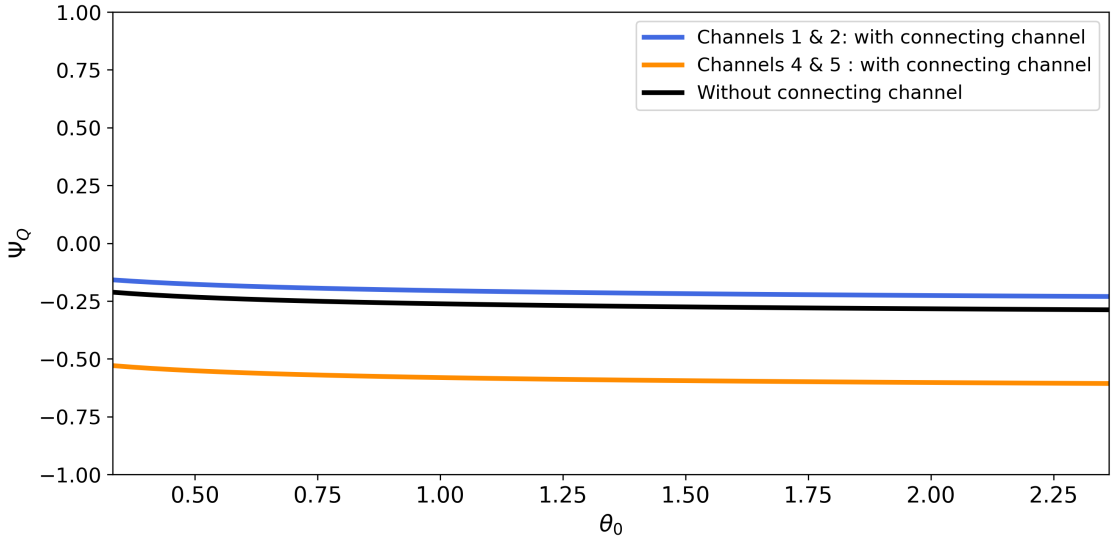

Figure 3.22: The discharge asymmetry between the downstream channels of the Wake Lake Delta plotted for a range of Shields stresses. The black line is the discharge asymmetry without connecting channel, the blue line is the discharge asymmetry between channels 1 and 2 and the orange line is the discharge asymmetry between channels 4 and 5. The starting dimensions of the channels are given in Table 2.9 and the values of the used parameters are given in Table 2.4.

the channel does not change in depth. To conclude, it is a very complex system where many processes happen at the same time all influencing each other.

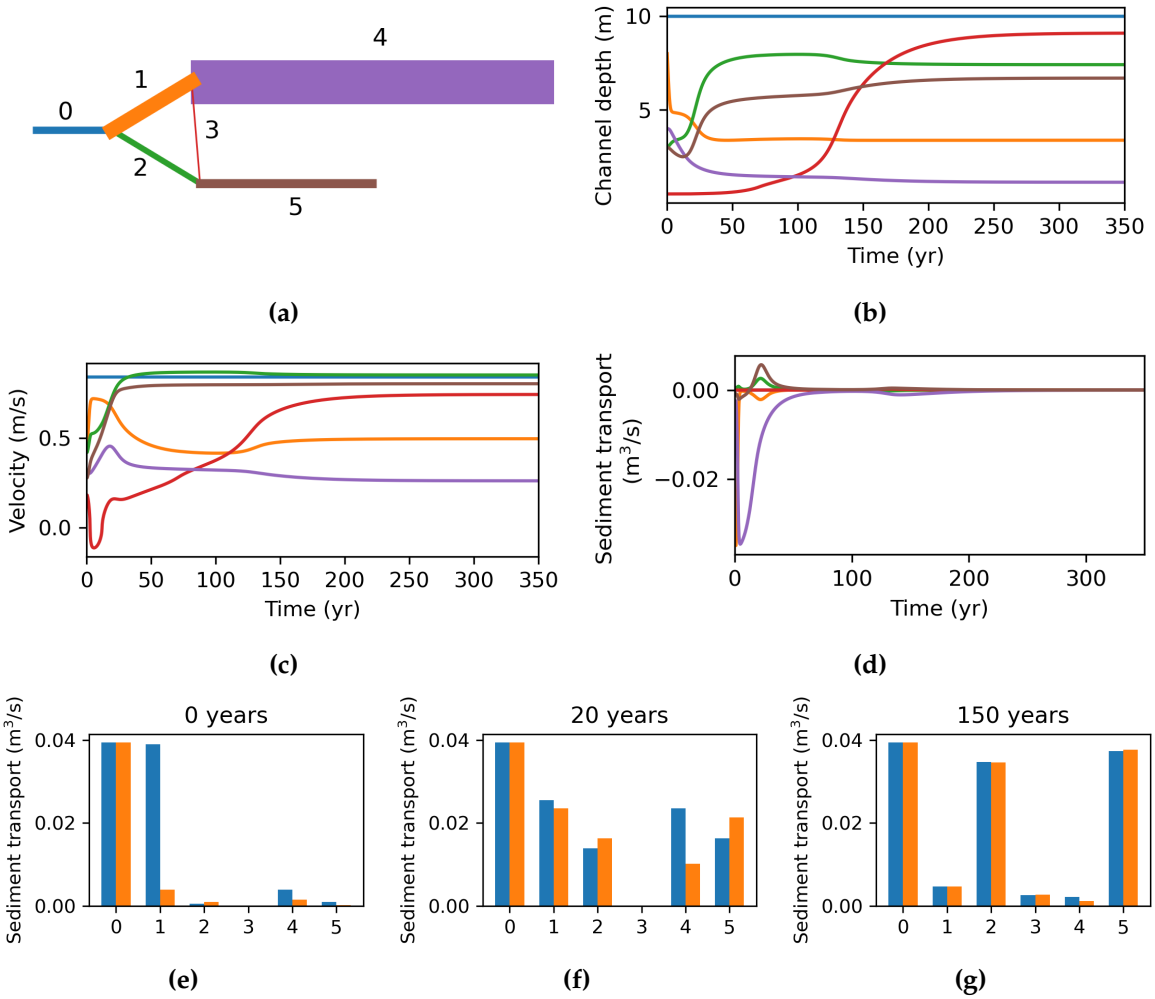

Figure 3.23: (a) Overview of the channel system. The width of the channels are correlated with widths of the lines. The blue line is channel 0, the orange line is channel 1, the line channel is channel 2, the red line is channel 3, the purple line is channel 4 and the brown line is channel 5. (b) Plot of the channel depth over time. The channel which the colour correspondents with is given in (a). The discharge, $Qr = 2520\ \mathrm{m}^3/\mathrm{s}$. The starting dimensions of the channels are given in Table 2.9 and the values of the used parameters are given in Table 2.4. (c) as (b) but the velocity over time is plotted. (d) as (b) but the difference in sediment transport at the end and the start of the channel over time is plotted. A positive value results in erosion and a negative value results in sedimentation. (e), (f) and (g) show the sediment transport at the start, blue, and end, orange, of the channel at 0 years, 20 years and 150 years into the simulation respectively. The channel number is given below the plot.

4. Discussion

4.1 One-channel system

To research how the strength of the tides, the river discharge, the channel length and the channel depth influence the widening of the channel, three sets of simulations were done. The results indicate that higher tidal amplitudes lead to wider river mouths, but stronger river discharges can reduce this effect. This is true for river discharges above 950 m^3/s. River discharges that are lower show less widening of the channel. The length of the channel positively correlates with the widening of the channel mouth. A channel widens the most when the channel is 20 m deep. Having a deeper or shallower channel results in a channel that widens less.

Different methods can be used to predict the channel width like using empirical or physical equations or a model, as in this project. The discharge due to the river flow and the maximum discharge at low tide minus the discharge due to the river flow are separated when using hydraulic geometry as a predictor (Sassi et al., 2012; Hagen, 2022). Sassi et al. (2012) used the 51 cross-sections in the Mahakam Delta to fit the coefficients of the hydraulic relation for predicting the cross-section area, which resulted in a r^2 of 0.84. This is considerably higher than the r^2 of 0.39 found using the model used in this project. Hagen (2022) used the same dataset of 36 single-channel estuaries as in this project to fit the coefficient of the hydraulic relation for predicting the width. Resulting in a RMSE of 0.39 which is comparable to the RMSD of 0.41 found using the model. Using hydraulic geometry for predicting the channel width, the width of the channel mouth will always increase when the strength of the river discharge decreases which is not the case below a certain threshold. Creating a non-linear empirical equation for predicting the width based on the strength of the tidal and river flow could improve the accuracy when predicting the width. Nienhuis et al. (2018) used a physics-based equation relating the ratio between the tidal amplitude and the bed slope to the width of the channel mouth. The channel length and the widening of the channel mouth are linearly related according to Nienhuis et al. (2018). This is true for certain depths but not always the case. Incorporating a depth-dependent factor into the equation might improve the results. Even though using a 0D model may not be as accurate as using empirical or physical-based equations, it does give a good insight into the processes determining the width of a channel.

Others used 1D models to predict the width of channels under the influence of tides. When prescribing a convergent channel width and letting the depth evolve, the channel depth gets a concave shape with the deepest point close to the seaward boundary (Lanzoni et al., 2002; Bolla Pittaluga et al., 2015b). Having a concave bed slope lowers the attenuation

of the tidal wave resulting in relatively high tidal velocities at the landward boundary which in turn increases the sediment transport. At the found equilibrium geometry the maximum high and low tide velocities are almost constant over the whole channel. Having a depth constant over the whole channel as in this project, the same is found (see Fig. 3.7c and Fig. 3.10c). Van der Wegen et al. (2010) used a 2D model with bed slope and bank erosion effects. At the start of the simulation, the channel had a constant width and depth. In the first few centuries mainly the width evolved resulting in a convergent width. After multiple centuries also the depth started to evolve into a concave depth. The model used in this project could therefore be improved by adding a prescribed depth profile as is done with the width profile already. Also researching the influence of an evolving width and depth at the same time could lead to interesting results. To do this a decision needs to be made about the sedimentation or erosion distribution between the width and depth. The amount of sedimentation or erosion can be divided by the ratio between the surface areas, the velocity of the flow or using hydraulic geometry relationships. The model used may not have a depth varying in space but it is able to do many simulations at a relatively low computational cost which can give a better understanding of the dependence on the initial conditions, the forcings and the parameters used.

The model overestimates the widths of channels that are longer than 50 km. This is likely attributed to processes not accounted for within the model, resulting in an overestimation of sediment transport at the seaward boundary or an underestimation of sediment transport at the landward boundary. This could be due to having a friction factor that is too strong resulting in excessive attenuation of the tides traveling into the channel. The used drag coefficient is $1/13^2 \approx 0.0059$ corresponding with a Chezy coefficient of $13\sqrt{g}$. Taking measurements found and fitting them with a model resulted in drag coefficients between 0.00128 and 0.00232 in the Lower Hudson Estuary and the James River Estuary (Ullman et al., 1998; Li et al., 2004). Repeating the simulation for the Yagon/Bago Delta as in Figure 3.7 with $C_d = 0.001$ resulted in a modelled width of 10.2 km instead of 509 km. Having a good approximation of the drag coefficient can improve the results greatly. Being able to model specific deltas well is not needed for finding patterns and getting a better understanding of the system which was the main goal of this project.

When keeping the width constant in time and only letting the depth evolve, there is a critical e-folding length for which the model finds an equilibrium depth. For lower e-folding lengths the channel fills up. Todeschini et al. (2008) researched the morphodynamics of an embayment. They found that there is a maximum equilibrium length the embayment can have depending on the convergence length scale where longer channels are less convergent than shorter channels. I found a similar pattern where channels which are less convergent have to be deeper. They also found that for stronger tidal forcings, the equilibrium length becomes shorter. Schuttelaars et al. (2000) did a similar experiment as Todeschini et al. (2008).They also found that for stronger tidal forcings, the maximum equilibrium length becomes shorter. This is again also true for the depth. Stronger tidal forcings resulted in lower minimum equilibrium depths.

4.2 Branching channel system

The complexity of the system was increased by letting the channel branch into two. The system was again allowed to evolve in width. The found equilibrium widths were perturbed to get a better understanding of the influence of tides on the stability of the system. Having a depth that is allowed to evolve after the perturbation allows the system to become asymmetrical. Tides cause the system to be more symmetrical and stable for a bigger range of river discharges. When increasing the river discharge, the tides have less influence and the system becomes more like it would be without tides. When letting the width evolve after the perturbation, the system always stays close to being symmetrical independent of the strength of the tides and the river discharge.

To see if the model results are reliable, it is compared with results from the model used in Bolla Pittaluga et al. (2015a) and Iwantoro et al. (2021). They both looked at the stability of a branching river, so without any tidal forcings. Bolla Pittaluga et al. (2015a) used a different method for calculating the change in depth after a time step. This should only make a difference in the time scale in which the morphological changes take place but not in the final results. In Table 2.4 the used values for the parameters are given and in Table 2.5 the used starting dimensions of the channel network are given.

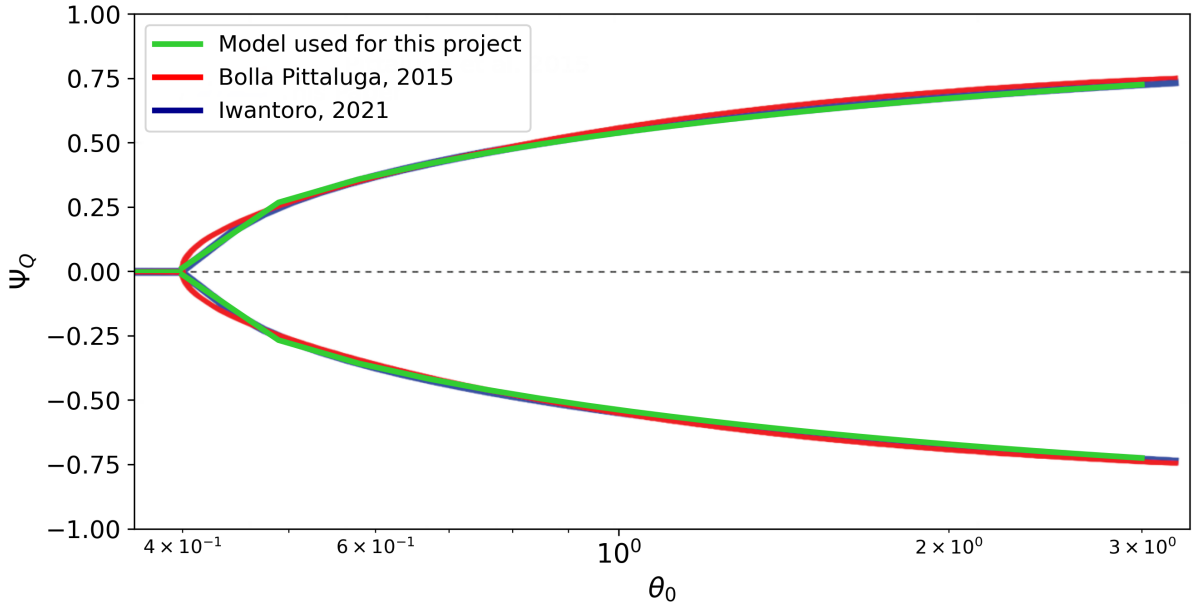

Figure 4.1: The discharge asymmetry plotted against the Shields stress with the same configurations as Bolla Pittaluga et al. (2015a), the red line and Iwantoro et al. (2021), the blue line. The values of the used parameters are given in Table 2.4 and the starting dimensions in Table 2.5. The results from the model used in this project, the green line, are plotted on top of Figure 5 from Iwantoro et al. (2021). The dotted grey line is the unstable symmetrical equilibrium solution.

The model used for this project gives results comparable to the models used in Bolla

Pittaluga et al. (2015a) and Iwantoro et al. (2021) (see Fig. 4.1). To be able to reproduce this result the friction factor had to be dependent on the channel depth when calculating the sediment transport. This was done by calculating the drag coefficient as shown below.

$$C_d = \left(\frac{1}{\log\left(\exp(1)\right)} / 0.4 * \log\left(\frac{12.2h}{0.035} \right) \right)^{-2}. \tag{4.1}$$

In the hydrodynamical part of the model, the drag coefficient, C_d, was assumed constant. Therefore I chose to always use a drag coefficient that is independent of the depth. The moment when the stable solutions of a branching river become asymmetrical shifts to lower Shields stresses when keeping the drag coefficient constant (see Fig. 4.2). Having a constant drag coefficient creates bigger discharge asymmetry at higher Shields stresses compared to having a drag coefficient that depends on the channel depth. Having a branching channel with perturbed depths, the drag coefficient that depends on the channel depth is relatively high for the shallow channel compared to the deeper channel. The sediment transport and the drag coefficient are related by: $Qs \propto {C_d}^{1.5}$, so having a higher drag coefficient causes an increase in sediment transport. This causes the channel to erode faster compared to having a drag coefficient that is independent of the depth. The opposite is true for the deeper channel, the drag coefficient is relatively low which causes low sediment transport and relatively high sedimentation. The relatively high erosion and sedimentation in the more shallow and deeper channel respectively makes the channel network stay longer in a symmetrical equilibrium and decreases the discharge asymmetry at higher Shields stresses.

The presence of an evolving width which has a stabilising effect on a branching channel could explain part of why there are so many stable branching channels in nature. Many researchers have studied the stability of a branching channel, but they only focused on the evolution of the channel depth, not its width (Bolla Pittaluga et al., 2003; Wang et al., 1995; Iwantoro et al., 2021; Redolfi et al., 2016; Edmonds et al., 2008). The results found may be a consequence of the decisions made about the widths of the downstream channels at the junction. I only researched two cases. The first one, where the widths stay constant and the second one where the widths are determined by the incoming and outgoing sediment transport. There are more possibilities like looking at only the incoming sediment transport or using hydraulic relationships. Using those methods could lead to different results where an evolving width does result in bigger discharge asymmetries. Hence, further research into the influence of an evolving width and the combination of an evolving width and depth on the stability of channel networks could lead to new insides.

The influence of tides causes the branching channel to stay longer symmetrical. Ragno et al. (2020) explained this by stating that tides cause a deepening of the channel which reduces the imposed asymmetry. The deepening of the channel also lowers the width-to-depth ratio which is in favor of the stability. Ragno et al. (2020) used a model that had a depth that was dependent on time and space and a width that was kept constant in time

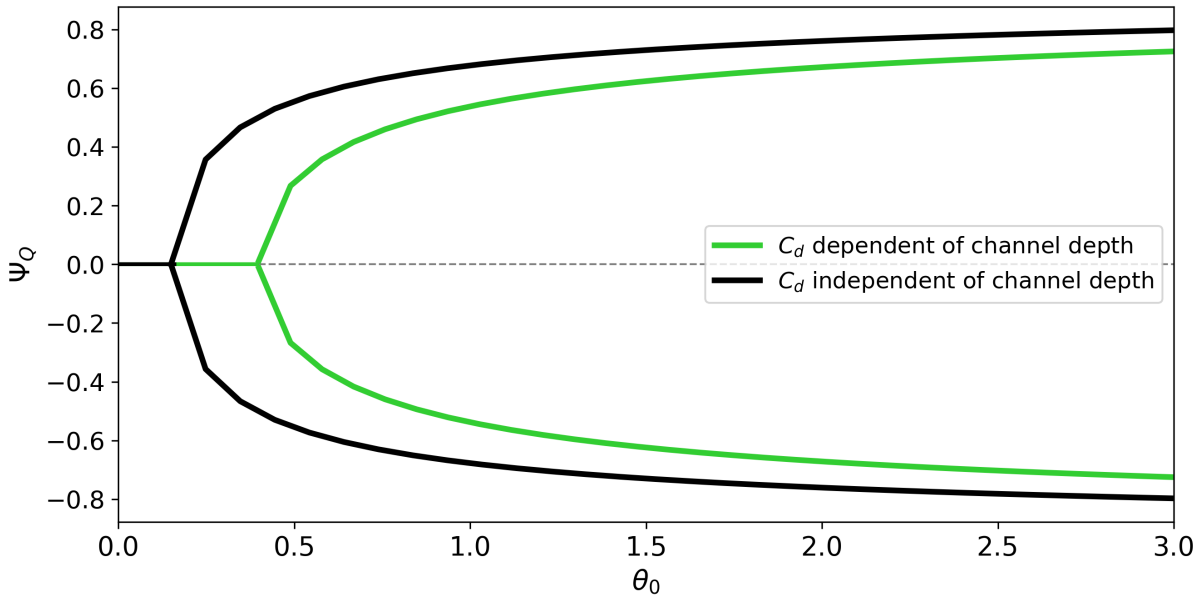

Figure 4.2: Discharge asymmetry plotted against the Shields stress with values of the used parameters in Table 2.4 and the starting dimensions in Table 2.5. The green line shows the results of the drag coefficient being dependent on the channel depth according to equitation 4.1. The black line shows the results with a constant $Cd = 1/13^2$. These are the same results as the black line in Fig. 3.12a but plotted against the Shields stress instead of the river discharge. The dotted grey line is the unstable symmetrical equilibrium solution.

and space. In the model used during this project, the width initially reaches an equilibrium before the depth is perturbed. The depth is then allowed to stabilize at an equilibrium level. Using this method, the channel depths before the perturbation are the same with and without tidal influence. The explanation of Ragno et al. (2020) can therefore not explain the stabilising effect of tides using this model. A new explanation is given in section 3.2.2. Iwantoro et al. (2022) found that the range of Shields stresses for which the network finds a symmetrical stable solution first grows for increasing u_2/u_0 before it becomes smaller again, where u_2/u_0 is the maximum semi-diurnal velocity divided by the residual velocity of the upstream channel at the junction. Early tests support these results. In the future, this could be researched more extensively. To research how well u_2/u_0 together with the Shields stress is as a predictor for the discharge asymmetry, u_2/u_0 and the discharge asymmetry after a perturbation in depth are calculated for the found equilibrium widths in Figures 3.8 and 3.9. Single simulations show a dependence that can be explained by looking at u_2/u_0 and the Shields stress but when plotting all simulations in one figure it becomes clear that u_2/u_0 and the Shields stress are not enough to predict the discharge asymmetry (see Fig. 4.3). It would be very useful to find a dimensionless parameter that can predict the discharge asymmetry. This parameter should include the Shields stress and u_2/u_0 but also other deciding factors.

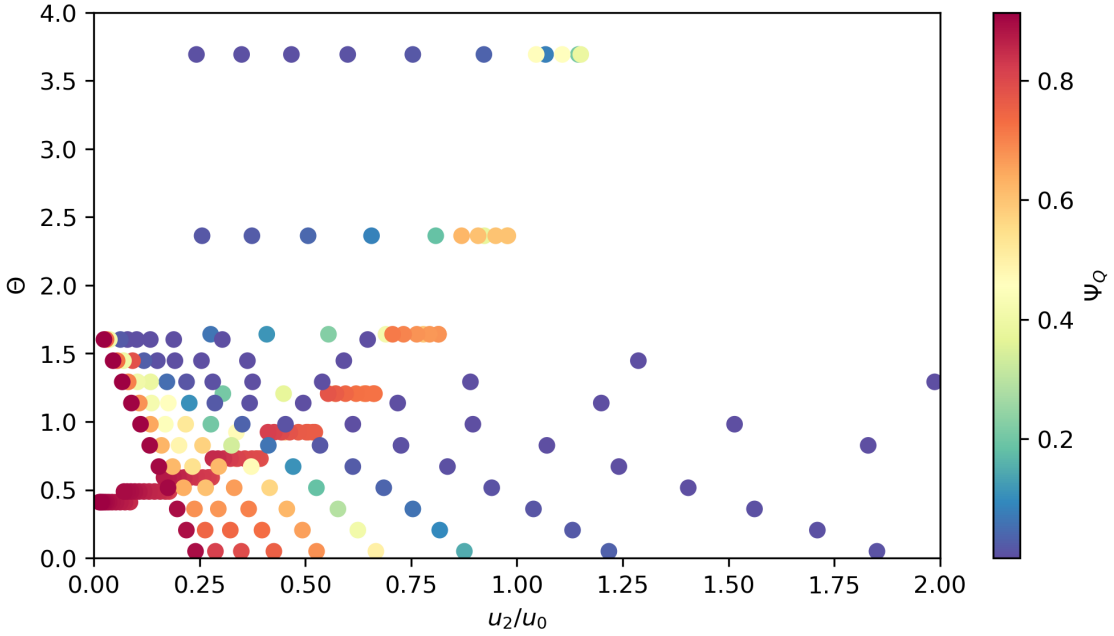

Figure 4.3: The Shields stress is plotted against u_2/u_0. The colour of the dot indicates the discharge asymmetry between the downstream channels. The channel system with equilibrium widths from Fig. 3.8 and Fig. 3.9 are perturbed in depth and the depth was allowed to evolve. u_2/u_0 is calculated before the perturbation.

4.3 Branching channel network with connecting channel without tides

Again the complexity of the system was increased by adding a connecting channel to the symmetrical branching channel system. This allowed periodic behaviour to form for a range of Shields stresses. The discharge asymmetry between channels 1 and 2, Ψ_{Q12}, is always closer to the discharge asymmetry of the downstream channels without connecting channel than the discharge asymmetry between channels 4 and 5, Ψ_{Q45}. The non-periodic solutions originate from two pitchfork bifurcations and the periodic solutions originate probably from a sub-critical Hopf bifurcation. When the connecting channel becomes smaller the bifurcation diagram looks more and more like the bifurcation diagram without the connecting channel.

Having Ψ_{Q12} always closer to the stable solution of the channel network without connecting the channel, compared to Ψ_{Q45} does give the impression that the connecting channel has more impact on the stable equilibrium solutions of channels 4 and 5 than of channels 1 and 2. Gao et al. (2023), who also inspired the use of this channel network, looked at the hydrodynamics of a symmetrical branching channel with a connecting channel. They found that Ψ_{Q12} is smaller and Ψ_{Q45} is larger in a network with a connecting channel than in a network without a connecting channel. They prescribed a water level difference of 0.5 m at the seaward boundary of channels 4 and 5 to create an asymmetry. To investigate if

the model used shows the same result, the discharge asymmetry is calculated before letting the depth evolve. Having a water level difference of 0.5 m is not a very realistic scenario, therefore instead of a water level difference a channel depth difference of 4 m between channels 4 and 5 is prescribed. Independent of the discharge, without the connecting channel the discharge asymmetry between the downstream channels is 0.149. With the connecting channel, the discharge asymmetry between channels 1 and 2 is 0.031 and between channels 4 and 5 is 0.266. This supports the findings of Gao et al. (2023). After the depth evolution, the discharge asymmetry does not show the same pattern. Not only we took the next logical step of studying the morphodynamics of this channel network but also Gao et al. (2024). They found similar discharge distributions and periodic behaviour when letting the channel depth evolve.

The bifurcation diagram starts to look more and more like the bifurcation diagram of a channel network without a connecting channel when the width of the connecting channel becomes smaller. Even with a connecting channel that is very small, 10 m, there is periodic behaviour visible. The maximum discharge asymmetry of the periodic behaviour is close to 0, meaning that the fluctuations in channel depth are very small and could be overlooked when taking measurements. It poses an intriguing question of whether there exists a threshold of the width of the connecting channel at which the periodic behaviour disappears or if this behaviour persists regardless of the width of the connecting channel.

During the simulation, the channel network used was symmetrical. In nature, all channels have different lengths, widths, depths, etc. To find out if the periodic behaviour is still there when the channel network is asymmetrical the width and length of channel 4 were varied for a river discharge of $Qr = 2450\ m^3/s$ which is in the middle of the stable periodic equilibrium solutions. The width of channel 4 was varied between 150 and 200 m in steps of 5 meters. The length of channel 4 was varied between 1 and 1.1 km in steps of 10 meters. The same was done but then changing channel 1 to see if it mattered if the asymmetry was upstream or downstream of the connecting channel. The percentual change in width and depth is calculated by $\Delta b\% = \frac{\Delta b}{b_i} * 100\%$ and $\Delta L\% = \frac{\Delta L}{L_i} * 100\%$ where Δb and ΔL are the change in width and length and b_i and L_i are the width and length of channel 2 or 5. Channels 2 and 5 are the reference channels for channels 1 and 4 respectively. The periodic behaviour stops when channel 1 is around 20% wider than channel 2 or when channel 4 is around 24% wider than channel 5 (see Fig. 4.4). When the length is changed the difference between channels 1 and 2, around 6%, is smaller than the difference between channels 4 and 5 that need a 8% difference. The change in length and depth wherefore the network is not periodic anymore is linearly related to each other. The Wax Lake Delta is an example found in nature where the channel system is not symmetrical. Letting the depth evolve resulted in complex behaviour which ended in channels 2 and 5 becoming the deepest channels. Between 1998 and 2012 mainly channels 0, 1 and 4 became deeper which is the opposite of what the model predicted (Meselhe et al., 2021). This could be because of the simplifications made like adding multiple channels together. Meselhe et al. (2021) show that the Wax Lake Delta grows 60 to 80 m/yr. Growing this fast takes a lot of sediment. Therefore it would be

possible that the incoming sediment is used for growing in length instead of becoming more shallow. To be able to capture this in the model floodplains should be added. A decision needs to be made on how sedimentation takes place on the floodplains. During the growth of the Wax Lake Delta, new mouthbars were formed. In the model, this could be added using a parameterisation.

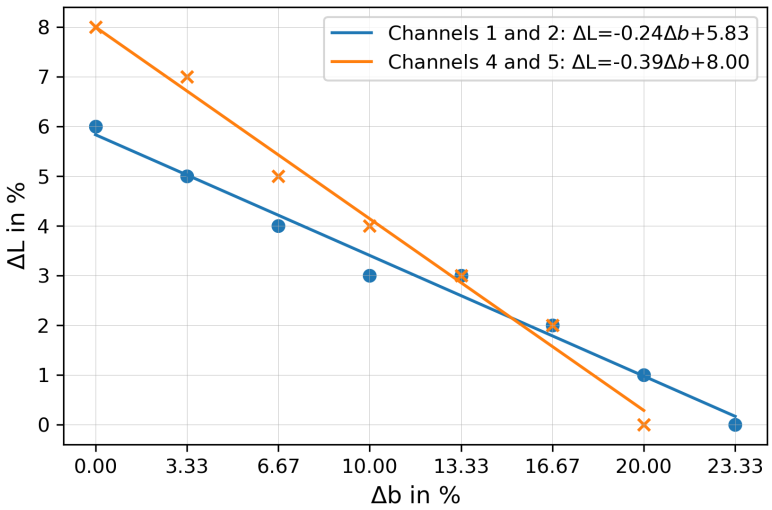

Figure 4.4: The change in length and width between the downstream channels needed to not have periodic behaviour anymore for Qr = 2450 m^3/s. Values of the used parameters in Table 2.4 and the starting dimensions in Tables 2.8 and 2.7 option 1. The blue line shows the results of a change in length and width in channel 1 and the orange line shows the results of a change in length and width in channel 4.

So far, in the system with a connecting channel, only the depth was allowed to evolve. When having a time-dependent width multiple options are possible as discussed in section 4.2. In the connecting channel, the direction of the flow can go both ways, meaning that what is defined as the upstream boundary switches between both channel ends. Which channels the upstream channels and the downstream channels are depends on the direction of the flow. This could cause big jumps in channel widths when prescribing that the sum of the downstream width is the same as the width of the upstream channel at the junction. An option would be to keep the width of the connecting channel constant time and letting only the other channels evolve.

To conclude, the model is capable of finding similar results as more complex models. Some alterations could be made so that the model can also be used in researching other processes like the influence of tides on the width of a channel system with a connecting channel. Even though the model may not be accurate when looking at specific deltas it is beneficial in researching the sensitivity to different parameters, forcings, and starting geometries.

5. Conclusions

The main aim was to understand how tides and river discharge determine the width and depths of deltaic channel systems. Three different systems were researched: a one-channel system, a branching channel system and a branching channel system with a connecting channel. The research questions connected to each channel system are:

1. How does the widening of a channel under the influence of tides depend on the strength of the tides, the river discharge, the channel depth and the channel length?
2. How do tides influence the stability of a branching channel with a varying width or depth?
3. What is the difference in stability between a branching channel with and without a connecting channel?

A 0D morphodynamical model is used to answer the research questions. The model is not great at predicting the morphodynamics of specific channel systems found in nature but it is a simple model with a low computational time making it easy to research a wide variety of settings to get a better understanding of the processes determining the evolution of the channel system.

The results of the one-channel system indicate that higher tidal amplitudes lead to wider river mouths, but stronger river discharges can reduce this effect. This is true for river discharges above 950 m3/s. River discharges that are lower show less widening of the channel mouth due to the low influence of the residual flow on the sediment transport at the landward boundary. The length of the channel positively correlates with the widening of the channel mouth because in a longer channel, the friction has a more impact on the tidal wave. A channel widens the most when the channel is 20 m deep. Having a deeper or shallower channel results in a channel that widens less. This is caused by the interaction of the residual velocity, which becomes lower for deeper channels, and the tidal velocity, which becomes higher for deeper channels.

In a branching channel system, the equilibrium widths are similarly dependent on the river discharge, tidal amplitude, channel length and channel width as in a one-channel system. The channels were perturbed to research the stability of the channel system. Having a depth that is allowed to evolve after the perturbation allows the system to become asymmetrical. Tides cause the system to be more symmetrical and stable for a bigger range of river discharges. Researching the stability of the equilibrium widths instead of equilibrium depths, a new explanation is found for why tides have a stabilising effect. When increasing the river discharge, the tides have less influence and the system becomes more like it would be without tides. When letting the width evolve after the perturbation, the system always

stays close to being symmetrical independent of the strength of the tides and the river discharge. During this project, the widths of the downstream channels at the junction were kept constant or dependent on the difference in outgoing and incoming sediment transport. There are other ways to determine the channel widths at the junction which could lead to different results. Therefore more research is needed.

Adding a connecting channel to the branching channel system increases the discharge asymmetry between the downstream channels at low Shields stresses and decreases the discharge asymmetry at high Shields stresses. For moderate Shield stresses stable periodic behaviour occurs. The discharge asymmetry between channels 1 and 2, is always closer to the discharge asymmetry of the downstream channels without connecting channel than the discharge asymmetry between channels 4 and 5. More research needs to be done to find out what causes the periodic behaviour because it could be due to choices made in the parameterization. The non-periodic solutions originate from two pitchfork bifurcations and the periodic solutions originate probably from a sub-critical Hopf bifurcation. When the connecting channel becomes smaller the bifurcation diagram looks more and more like the bifurcation diagram without the connecting channel.

Bibliography

Alebregtse, NC and HE De Swart (2016). "Effect of river discharge and geometry on tides and net water transport in an estuarine network, an idealized model applied to the Yangtze Estuary". In: *Continental Shelf Research* 123, pp. 29–49.

Bolla Pittaluga, M, G Coco, and MG Kleinhans (2015a). "A unified framework for stability of channel bifurcations in gravel and sand fluvial systems". In: *Geophysical Research Letters* 42.18, pp. 7521–7536.

Bolla Pittaluga, M, R Repetto, and M Tubino (2003). "Channel bifurcation in braided rivers: Equilibrium configurations and stability". In: *Water Resources Research* 39.3.

Bolla Pittaluga, Michele et al. (2015b). "Where river and tide meet: The morphodynamic equilibrium of alluvial estuaries". In: *Journal of Geophysical Research: Earth Surface* 120.1, pp. 75–94.

Buschman, FA et al. (2013). "Water and suspended sediment division at a stratified tidal junction". In: *Journal of Geophysical Research: Oceans* 118.3, pp. 1459–1472.

Cohen, Sagy et al. (2013). "WBMsed, a distributed global-scale riverine sediment flux model: Model description and validation". In: *Computers & Geosciences* 53, pp. 80–93.

Cowan, Carolyn (2023). *As hydropower dams quell the Mekong's life force, what are the costs?* https://news.mongabay.com/2023/03/as-hydropower-dams-quell-the-mekongs-life-force-what-are-the-costs/#:~:text=To%20date%2C%20more%20than%20160,either%20planned%20or%20under%20construction.. [Accessed 13-02-2024].

Edmonds, Douglas A and Rudy L Slingerland (2008). "Stability of delta distributary networks and their bifurcations". In: *Water Resources Research* 44.9.

Egbert, Gary D and Svetlana Y Erofeeva (2002). "Efficient inverse modeling of barotropic ocean tides". In: *Journal of Atmospheric and Oceanic technology* 19.2, pp. 183–204.

Eslami, Sepehr et al. (2019). "Flow division dynamics in the mekong delta: application of a 1D-2D coupled model". In: *Water* 11.4, p. 837.

Gao, Weilun et al. (2023). "Floodplain Connecting Channels as Critical Paths for Hydrological Connectivity of Deltaic River Networks". In: *Water Resources Research*, e2022WR033714.

Gao, Weilun et al. (2024). Unpublished paper.

Hagen, Reinet (2022). "The effect of sea-level rise on the equilibrium width of tide- and river dominated estuaries". Bachelor's Thesis. Utrecht: Untrecht University.

Hansen, Eggert and Frank A. Engelund (1972). *A monograph on sediment transport in alluvial streams*. Technical University of Denmark.

Hoitink, AJF and David A Jay (2016). "Tidal river dynamics: Implications for deltas". In: *Reviews of Geophysics* 54.1, pp. 240–272.

Iwantoro, AP, M van der Vegt, and MG Kleinhans (2020a). "Morphological evolution of bifurcations in tide-influenced deltas". In: *Earth Surface Dynamics* 8.2, pp. 413–429.

Iwantoro, AP, M van der Vegt, and MG Kleinhans (2021). "Effects of sediment grain size and channel slope on the stability of river bifurcations". In: *Earth Surface Processes and Landforms* 46.10, pp. 2004–2018.

Iwantoro, AP, M van der Vegt, and MG Kleinhans (2022). "Stability and asymmetry of tide-influenced river bifurcations". In: *Journal of Geophysical Research: Earth Surface* 127.6, e2021JF006282.

Iwantoro, AP et al. (2020b). "Effect of tides on stability of bifurcations in river deltas". In: *River Flow 2020*, pp. 464–468.

Lanzoni, Stefano and Giovanni Seminara (2002). "Long-term evolution and morphodynamic equilibrium of tidal channels". In: *Journal of Geophysical Research: Oceans* 107.C1, pp. 1–1.

Li, Chunyan et al. (2004). "Estimation of drag coefficient in James River Estuary using tidal velocity data from a vessel-towed ADCP". In: *Journal of Geophysical Research: Oceans* 109.C3.

Meselhe, Ehab, Kazi Sadid, and Ashok Khadka (2021). "Sediment distribution, retention and morphodynamic analysis of a river-dominated deltaic system". In: *Water* 13.10, p. 1341.

Mikhailov, VN (1970). "Hydrologic-morphometric characteristics of delta branches". In: *Stud. Rep. Hydrol* 9, pp. 146–158.

Nienhuis, Jaap H, AJF Hoitink, and Torbjörn E Törnqvist (2018). "Future change to tide-influenced deltas". In: *Geophysical Research Letters* 45.8, pp. 3499–3507.

Ragno, Niccolò, Nicoletta Tambroni, and Michele Bolla Pittaluga (2020). "Effect of small tidal fluctuations on the stability and equilibrium configurations of bifurcations". In: *Journal of Geophysical Research: Earth Surface* 125.8, e2020JF005584.

Redolfi, Marco, Guido Zolezzi, and Marco Tubino (2016). "Free instability of channel bifurcations and morphodynamic influence". In: *Journal of Fluid Mechanics* 799, pp. 476–504.

Rogers, Kimberly G et al. (2013). "Farming practices and anthropogenic delta dynamics". In: *Deltas: Landforms, Ecosystems and Human Activities, Redbook Proceedings of HP1, IAHS Publ* 358, pp. 133–142.

Rosen, Timothy and Y Jun Xu (2013). "Recent decadal growth of the Atchafalaya River Delta complex: Effects of variable riverine sediment input and vegetation succession". In: *Geomorphology* 194, pp. 108–120.

Rousseau, Jean-François and Melissa Marschke (2023). "(In) visible fluidities across sandscapes: Sand dredging and local socio-environmental impacts along the Red and Mekong Rivers". In: *The Extractive Industries and Society* 14, p. 101261.

Safra de Campos, Ricardo et al. (2020). "Where people live and move in deltas". In: *Deltas in the Anthropocene*, pp. 153–177.

Sassi, Maximiliano G et al. (2012). "Downstream hydraulic geometry of a tidally influenced river delta". In: *Journal of Geophysical Research: Earth Surface* 117.F4.

Sassi, Maximilliano Gabriel (2013). *Discharge regimes, tides and morphometry in the Mahakam delta channel network*. Wageningen University and Research.

Schuttelaars, HM and HE De Swart (2000). "Multiple morphodynamic equilibria in tidal embayments". In: *Journal of Geophysical Research: Oceans* 105.C10, pp. 24105–24118.

Shaw, John B, David Mohrig, and Spencer K Whitman (2013). "The morphology and evolution of channels on the Wax Lake Delta, Louisiana, USA". In: *Journal of Geophysical Research: Earth Surface* 118.3, pp. 1562–1584.

Soulsby, Richard (1997). "Dynamics of marine sands". In.

Syvitski, James PM and Yoshiki Saito (2007). "Morphodynamics of deltas under the influence of humans". In: *Global and Planetary Change* 57.3-4, pp. 261–282.

Todeschini, Ilaria, Marco Toffolon, and Marco Tubino (2008). "Long-term morphological evolution of funnel-shape tide-dominated estuaries". In: *Journal of Geophysical Research: Oceans* 113.C5.

Ullman, David S and Robert E Wilson (1998). "Model parameter estimation from data assimilation modeling: Temporal and spatial variability of the bottom drag coefficient". In: *Journal of Geophysical Research: Oceans* 103.C3, pp. 5531–5549.

Van der Wegen, M, A Dastgheib, and JA Roelvink (2010). "Morphodynamic modeling of tidal channel evolution in comparison to empirical PA relationship". In: *Coastal Engineering* 57.9, pp. 827–837.

Wang, Zheng Bing et al. (1995). "Stability of river bifurcations in ID morphodynamic models". In: *Journal of Hydraulic research* 33.6, pp. 739–750.

Woodroffe, Colin D et al. (2006). "Landscape variability and the response of Asian megadeltas to environmental change". In: *Global change and integrated coastal management: The Asia-Pacific region*, pp. 277–314.

A. Used variables and parameters and their units

α	factor over which transverse sediment transport takes place	
b	channel width	m
C_d	drag coefficient	
$d50$	median diameter sediment	m
η	free surface elevation	m
$\mathcal{N}$	complex amplitude	
ϕ	tidal phase at boundary channel network with the ocean	rad
g	gravitational acceleration	m/s^2
γ	inverse convergence length	m^{-1}
h	channel depth	m
κ	complex wave number	
L	channel length	m
λ	effective friction coefficient	m/s or dimensionless
N	tidal amplitude at boundary channel network with the ocean	m
p	porosity	
Ψ_Q	Discharge asymmetry	
Qr	river discharge	m^3/s
Qs	sediment transport	m^3/s
r	calibration parameter transverse sediment transport	
s	relative density sediment	
σ	tidal frequency	s^{-1}
t	time	s
θ	Shields stress	
u	total velocity	m/s
$\mathcal{U}$	complex velocity	
V	channel volume	m^3
x	along channel distance	m

B. Overview simulations

Set of simulations	Perturbation in	Changing width/depth	$\mathbf{b}_0$
1	depth	depth	constant
2	depth	depth	changing
3	depth	width	constant
4	depth	width	changing
5	width	width	constant
6	width	width	changing
7	width	depth	constant
8	width	depth	changing

Table B.1: Overview of all sets of simulations done for research question 2.

C. Data

Name	Lat	Lon	Q_{river} (m^3/s)	h (m)	L (m)	N (m)	b_0 (m)	b_L (m)
Arno	43.6	10.3	57	2.0	5.9E+3	0.35	80	125
Brazos	28.9	-95.4	189	2.9	2.2E+4	0.35	150	230
Ceyan	36.6	35.6	222	3.0	1.3E+4	0.35	111	150
Colorado (TX)	28.6	-96.0	76	2.2	1.7E+4	0.35	107	131
St George, Danube	44.9	29.6	1500	5.4	6.9E+4	0.025	400	470
Ebro	40.7	0.8	600	4.1	2.2E+4	0.1	235	315
Eel	40.6	-124.3	235	3.1	4.3E+3	1.5	103	300
Huanghe	37.7	118.8	1480	5.4	6.7E+4	0.4	550	800
Indus	25.5	68.3	3171	6.7	1.3E+5	2.5	613	2500
Klamath	41.5	-124.1	473	3.8	5.1E+3	1.5	170	240
Limpopo	-25.2	33.5	835	4.5	4.5E+4	0.6	405	550
Magdalena	11.0	-74.8	7530	8.7	8.9E+4	0.5	900	910
Orange	-28.6	16.5	442	3.7	1.7E+4	0.75	210	228
Pescara	42.5	14.2	29	1.6	3.2E+3	0.3	37	38
Squamish	49.7	-123.2	250	3.1	4.0E+3	1.5	110	200
Var	43.7	7.2	41	1.8	4.8E+2	0.25	75	80
Vistula (Wisla)	54.3	18.9	1050	4.8	3.7E+4	0.5	400	472
Waipaoa	-38.7	177.9	41	1.8	1.4E+3	0.6	110	120
Pericuma	-2.4	-44.9	115	2.5	5.0E+4	3.675	100	1500
Maracana	-0.9	-47.5	238	3.1	6.2E+4	3	180	2058
Marapanim	-0.8	-47.7	186	2.9	5.8E+4	3.035	189	2954
Cacipore	3.6	-51.2	514	3.9	7.8E+4	2.015	200	4000
Suriname	5.8	-55.2	440	3.7	3.7E+4	1.385	557	2000
Demerara	6.9	-58.2	300	3.3	3.3E+4	1.56	200	900
Sungai Merauke	8.5	140.3	330	3.4	5.7E+4	1.56	90	900
Mahi	22.3	72.8	380	3.6	8.9E+4	5.46	342	11505
Purna	21.0	73.0	120	2.5	1.3E+4	3.23	98	1126
Kumbe	8.4	140.2	144	2.7	2.7E+4	1.9	96	330
Yangon/Bago	16.6	96.6	3887	7.2	2.8E+5	2.025	800	6694
Bilin	17.2	97.3	1490	5.4	3.6E+4	2.405	245	3200
Sokyosen	36.9	126.9	1500	5.4	5.4E+4	5.425	236	3200
Taeryong	39.6	125.4	700	4.3	4.8E+4	3.365	435	2500
Yoneshiro	40.3	140.1	250	3.1	3.1E+4	0.155	160	450
Wai Bian	-8.2	140.0	208	3.0	2.5E+4	3.145	114	2500
Weser	53.6	8.6	288	3.3	6.6E+4	1.705	150	1500
Thames	51.5	0.6	65	2.1	7.2E+4	3.74	70	6618
Ombrone	42.7	11.1	31	1.7	4.2E+3	0.215	73	116
Tibre	41.8	12.3	70	2.1	7.2E+3	0.22	136	162

Table C.1: Data of single channels in deltas from the data set of Nienhuis et al., 2018.